Master's Thesis

Cell design/fabrication and optimization of cell components for rechargeable all-liquid metal batteries

Junsoo Kim

Department of Energy Engineering

(Battery Science and Technology)

Graduate School of UNIST

2017

Cell design/fabrication and optimization of cell components for rechargeable all-liquid metal batteries

Junsoo Kim

Department of Energy Engineering

(Battery Science and Technology)
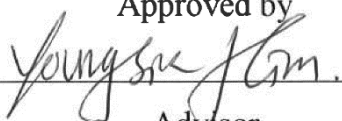
Graduate School of UNIST

Cell design/fabrication and optimization of cell components for rechargeable all-liquid metal batteries

A thesis/dissertation

submitted to the Graduate School of UNIST

in partial fulfillment of the

requirements for the degree of

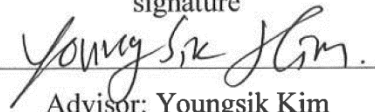Master of Science

Junsoo Kim

01. 11. 2017
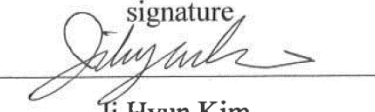
Approved by

Advisor

Youngsik Kim

Cell design/fabrication and optimization of cell components for rechargeable all-liquid metal batteries

Junsoo Kim

This certifies that the thesis/dissertation of Junsoo Kim is approved.

01. 11. 2017

signature

Advisor: Youngsik Kim

signature

Ji Hyun Kim

signature

Seok Ju Kang

Contents

Abstract

Energy storage systems (ESSs) have recently received great attention to store electrical energy genergated from renewable resources such as solar, wind, and waves. Among ESSs, electrochemical energy storage devices (EESDs) such as Li-ion and Na-S batteries have been considered as promising candidates due to its advantages of high energy density and coulombic efficiency. Recently, all-liquid metal batteries (LMBs) have been considered as one of the most powerful EESDs due to their high rate capability, ease of scaling up, long lifespan, and low cost. Neverthelss, researches on cell design and fabricaton of the LMBs have not been fully reported, and this information is critical to testing new materials and identification of their potentials as new anode and cathode materials.

In this thesis, the cell components for LMBs were established through circulation from the following three steps: (i) cell design/fabrication, (ii) assembly, and (iii) electrochemical testing. The cell design and its components have been changed and updated after many trials and errors. The cells with compositions of Li|LiCl-LiF|Bi cell was assembled and tested at 50 and 100 mA at 540 ^{o}C. It exhibited a relatively long-term cycling at 50 mA. In the updated cell, the Li|LiCl-LiF|Bi cell showed good cycling performance at the current of 100 mA and 200mA at 560 ^{o}C. In addition, the Li|LiCl-LiI|Bi-Pb cell demonstrated an excellent long-term cycling stability (>750 cycles (~150 days)) and high coulombic efficiency of >99.3% at 500 mA at 410 ^{o}C. Future plans about further optimization of testing cells and development of new chemistries for low-temperature, long-term operation will be discussed

List of figures

of Li|LiCl-LiF|Bi LMB cell during heat up to 560 $^{\circ}$C in (a) and (b) is the result of galvanostatic cycling at 100 mA (560 $^{\circ}$C).

Figure 42. Electrochemical performance of Li|LiCl-LiF|Bi LMB cell. (a) shows change of charge and discharge capacity and coulombic efficiency during cycling and (b) is the OCV after 30 minutes after charge and discharge.

Figure 43. Electrochemical performance of Li|LiCl-LiF|Bi LMB cell. The open circuit voltage change of Li|LiCl-LiF|Bi LMB cell during heat up to 560 $^{\circ}$C in (a) and (b) is the result of galvanostatic cycling at 200 mA (560 $^{\circ}$C).

Figure 44. Electrochemical performance of Li|LiCl-LiF|Bi LMB cell. (a) shows change of charge and discharge capacity and coulombic efficiency during cycling and (b) is the OCV after 30 minutes after charge and discharge.

Figure 45. Expected problems of Li|LiCl-LiF|Bi LMB cell. (a) Cross section of Li|LiCl-LiF|Bi LMB cell and (b) actual image after Li soaking.

Figure 46. Images of (a) comercialized Ni-Fe foam, (b) Ni-fe foam combined with negative current collector using thread and nut, and (c) surface and cross section after Li soaking.

Figure 47. The results of TGA and DSC on (a) LiI and (b) LiCl salt. In result of (a), 80.32 $^{\circ}$C, 132.21 $^{\circ}$C, and 320.07 $^{\circ}$C as endothermic reaction mean removing of moisture and residue organic waste. In result of (b), 79.73 $^{\circ}$C, also, means removing of moisture.

Figure 48. The results of TGA and DSC on manufactured LiCl-LiI salt. 66.23 $^{\circ}$C, 77.60 $^{\circ}$C, and 127.75 $^{\circ}$C as endothermic reaction mean removing moisture and residue organic waste. Endothermic reaction at 368.63 $^{\circ}$C means melting point of LiCl-LiI.

Figure 49. Electrochemical performance of Li|LiCl-LiI|Bi-Pb LMB cell. The open circuit voltage change of Li|LiCl-LiI|Bi-Pb LMB cell during heat up to 410 $^{\circ}$C in (a) and (b) shows voltage profiles, which is 1st, 20th, 30th, 40th, and 86th, of discharge and charge at 500 mA (410 $^{\circ}$C).

Figure 50. Change of charge and discharge capacity and coulombic efficiency of Li|LiCl-LiI|Bi-Pb LMB cell during cycling.

Figure 51. The result of cool down test of Li|LiCl-LiI|Bi-Pb. (a) shows coulobic efficiency and change

Figure C-3. Manufactured LiCl-LiI salt using quartz tube.

List of tables

1. Introduction

1.1. Electrical energy storage(EES) systems

Resource of electric power production grows in importance while demand of it continuously increases. The amount of its production runs to nearly 22,200 TWh and 70 % of that depends on fossil fuels.[1] A high level of dependence on it causes a lot of carbon dioxide gas release which is a main reason of generating global warming. For reducing its release, research and development of alternative energy resources are necessity for resolving a mentioned conflict.[2] Solar, wind, tides, waves, and geothermal heat, which are considered as environment-friendly and renewable energy resources, come to the fore as alternative.

Electrical energy, which is generated from power plant using renewable source, is supplied to industry, commerce, household, etc. As shown in Figure 1, renewable resource is fluctuated dependence on geographical position and weather. In response to that, the amount of electrical energy is also fluctuated.[3] When considering generated electrical energy directly transmits to consumers, if amount of generated electrical energy is higher than demand of consumers, dump power, which is remained electrical energy after consumers use, is thrown out. In the opposite case, the blackout comes up. To solve these problems which is caused by intermittency of renewable resource, electrical energy storage devices (EESDs) or system, which transmit electrical energy to consumers after storing dump power, are designed as shown in Figure 2.[3, 4, 5, 6]

To smooth out the intermittency of renewable energy production, low-cost EESDs have brought research attention such as batteries, pumped hydro, compressed air energy storage, high-power flywheels, and supercapacitor.[3, 7] Additionally, Smart grid technologies contribute to easily balancing between EES system and consumers.[8] Following research attention, batteries are considered as attractive candidates owing to their long cycle life, high energy

density, high coulombic efficiency, and flexibility for large-scale EESDs such as redox flow batteries[9], sodium-sulfur batteries[10], sodium-metal halide batteries[11], Li-ion batteries[12], and lead-acid batteries[13]. In next section, a brief description will be explained such as structure, benefits, shortcoming, etc.
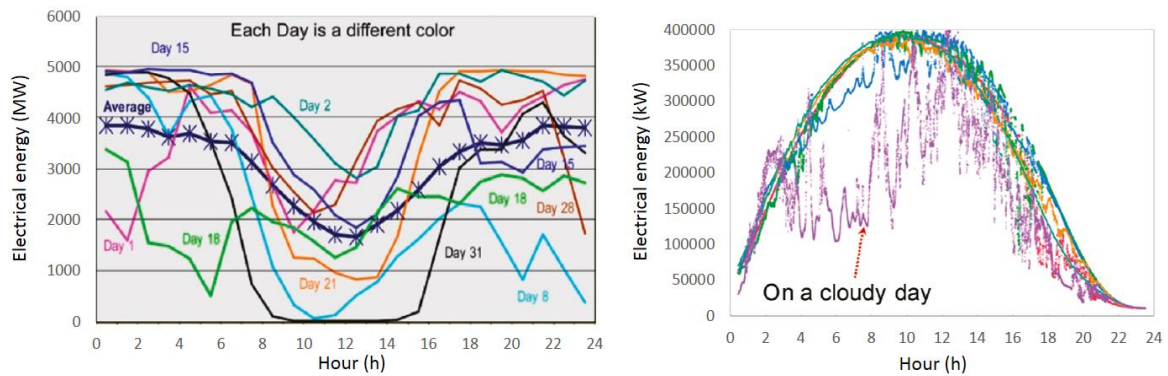
Figure 1. Electrical energy generated from wind(left) and solar(right) as renewable resource.[3]
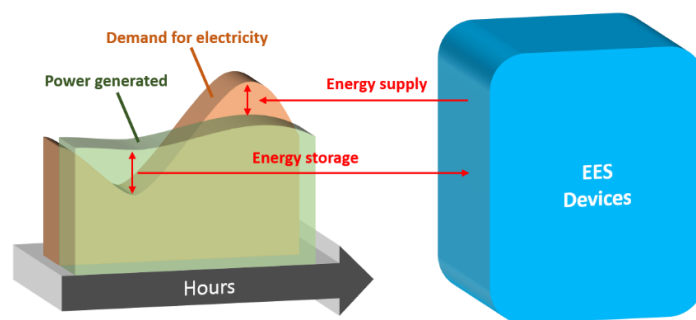
Figure 2. Schematic of fluctuation of power generated from power plants and demand for electrical energy along to time and role of Electrical energy storage devices as load leveling.

1.2. Electrochemical energy storage devices (EESDs)

Redox flow batteries (RFBs) have been well known as EESDs.[3, 9] There were many types of researched redox couple for RFBs such as ion-chromium (Fe-Cr), all vanadium, vanadium-bromine (V-Br), etc. Among these variety of RFBs, a lot of research on vanadium redox flow batteries(VRFB) have proceeded.[11, 12, 13, 14] As shown in Figure 3, structure of all vanadium redox flow battery is described.[3] It is composed of positive and negative electrode, catholyte, anolyte, ion-selective membrane, and pump for both electrolyte. Overall the reaction is as follows.

$$\text{Overall reaction: } VO_2^+ + V^{2+} + 2H^+ \Leftrightarrow VO^{2+} + V^{3+} + H_2O$$
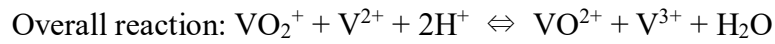
Its benefits are flexibility, high coulombic efficiency, long cycle life, scalability, etc.[9]
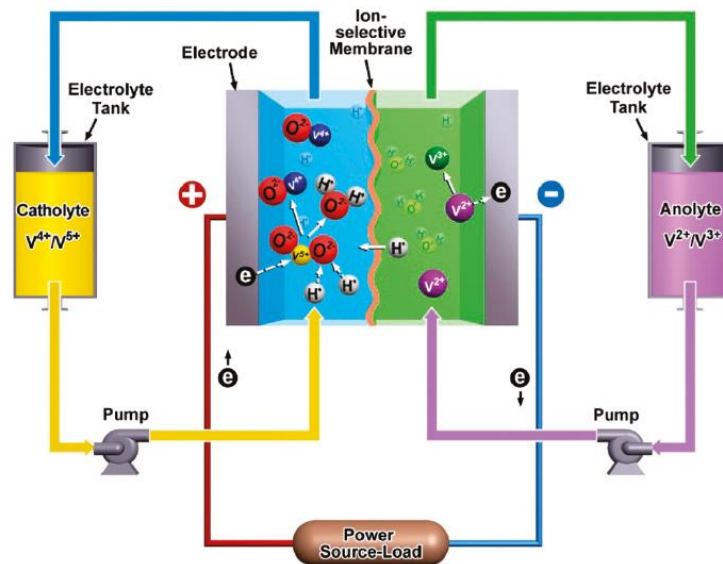
Figure 53. Constitution of all vanadium redox flow battery.[3]

Sodium-sulfur (Na-S) batteries has many advantages such as being low cost, easily mass production, no emissions, and 99 % of its weight is recycled.[17] As shown in Figure 4, the illustration of Na-S batteries is described. Na-S batteries are usually operated at 350 ℃ and consist of sodium as negative electrode, sulfur as positive electrode, and beta-alumina for electrolyte. Sodium ions are traveling back and forth through the electrolyte during charge and discharge. Discharge and charge mechanism is based on two electron change reaction as follows.

$$\text{Anode interface: } 2Na \Leftrightarrow 2Na + 2e^-$$

$$\text{Cathode interface: } XS + 2e^- \Leftrightarrow S_X^{2-}$$
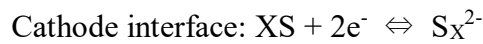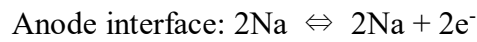
In case of practical field, a 34 MW/ 238 MWh Na-S system was under construction in Rokkasho wind farm in northern, Japan.[3]
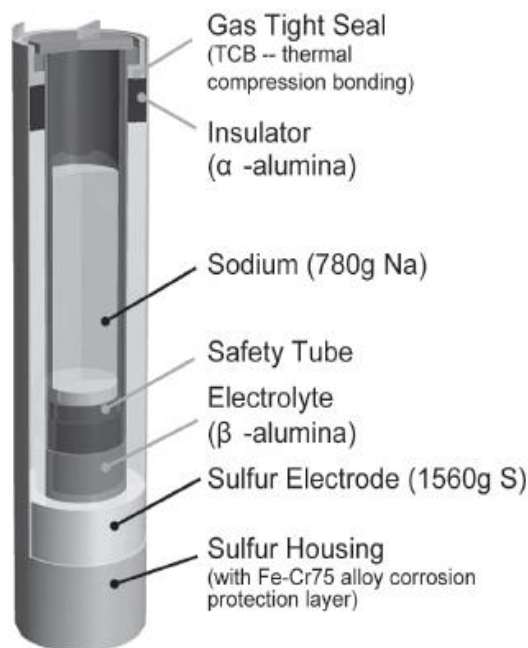
Figure 4. Schematic of sodium-sulfur battery cell developed by NGK insulators, LTD.[10]

Li-ion batteries(LIBs) have been widely investigated from the 1970s. Generally, it consists of solid state materials for anode and cathode, ionic conductive liquid state electrolyte, separator, etc. Many studies that aimed at portable devices have been published due to their high energy and power density, high coulombic efficiency, etc. [17, 18, 19] These benefits help to move interest to EESDs. [3] For example, promising LIB for EESD was reported as using TiO_2-based electrode. [20]

Such conventional batteries are probably not suitable for a quick charge and discharge at the megawatt level such as frequency regulator[21] because of their low current rate in a practical field. Solid components of them, such as $LiCoO_2$ (ionic conductivity: 5.5×10^{-4} s cm^{-1}) and graphite for LIBs, beta alumina (Na, β"-Al_2O_3, ionic conductivity: 1.0×10^{-1} s cm^{-1}) for NaS batteries, etc, have lower ionic conductivity than liquid components because mobile ions do not easily move in solid components.[22, 23] While conventional batteries have these weak points, liquid metal batteries (LMBs), which are composed of all liquid state such as liquid metal as anode and cathode and molten salt as electrolyte, overcome low current rate due to fast ionic conductivity of molten salt (for example, ionic conductivity of LiF-LiCl-NaF: 3.44 s cm^{-1}).[24, 25] As an example, in previous reported paper, the current density of VRFB is 40 mA/cm^2 during charge and discharge.[15, 16] On the contrary, that of LMBs is, generally, 200 mA/cm^2 during processing.[51, 52, 54] Therefore, it is probably more suitable for quick charge and discharge applications. However, it was not widely investigated, therefore, in next section, the overview of LMBs will be introduced and explained.

1.3. Liquid metal batteries (LMBs)

1.3.1. Origin

The concept of LMBs is originated from three-liquid-layer cells. The hoopes cell, which consist of three-liquid-layer, was firstly developed as shown in Figure 5 for production of pure aluminum (Al) in 1922.[25] Anode, cathode, and electrolyte are pure Al, Al-Cu alloy, and AlF$_3$-NaF-BaF$_2$, respectively. It hasn't been used for batteries application, but only used to extract pure Al, in other words, from the perspective of electrochemistry, it only used charge reaction (Al $_{in\ Al-Cu\ alloy}$ $\rightarrow$ Al). Nevertheless, it has equal configuration as LMBs. In 1967, thermally regenerative bimetallic cells were examined in Argonne National Laboratory (ANL).[26] As shown, Figure 6 depicted by ANL, is divided into two parts, one is regenerator and the other is galvanic cell. In the regenerator part, liquid alloy composed of liquid metal anode (A) and cathode (B) are heated by heat source. Relatively volatile A will be vaporized at T$_2$ and then move to galvanic cell part through channel. In that part, the A vapor lose heat until being T$_1$ and it enters full of liquid metal A and then redox reaction occurs in anode (A $\rightarrow$ A$^+$ + e$^-$) and cathode (A$^+$ + e$^-$ $\rightarrow$ AC $_{in\ C}$) electrode. Considering galvanic cell part has three-liquid-layers and redox reaction, it also has same configuration as the LMBs. As one of the bimetallic cells, Figure 7 shows Na|NaF-NaCl-NaI|Na-Bi cell, which uses liquid sodium as anode, NaF-NaCl-NaI as electrolyte, and liquid sodium-bismuth alloy as cathode.[26] It accomplishes relatively high current of 50 A at 535-650 ^{o}C. During discharge, liquid Na will be oxidized and then move to Na-Bi electrode through liquid electrolyte. On the contrary, the reverse reactions occur on charging. In summary, Hoopes cell has the first three-liquid-layer structure using electrochemically extraction of pure Al. In ANL, thermally regenerative bimetallic cells were examined. Structure and operating mechanism is very similar to LMBs.

LMBs were researched by D. Shadoway et al in 2006. They focus on large-scale energy

storage using batteries. Through above mentioned research, they found positive possibility of use of liquid state materials for batteries due to their relatively ultra-fast rate capability, immunity to degradation of electrode, and, most of all, cost.[27] They established Ambri Inc, which manufactures LMBs for large-scale energy storage devices, as a partner. More details such as description and mechanism will be explained in the following section.
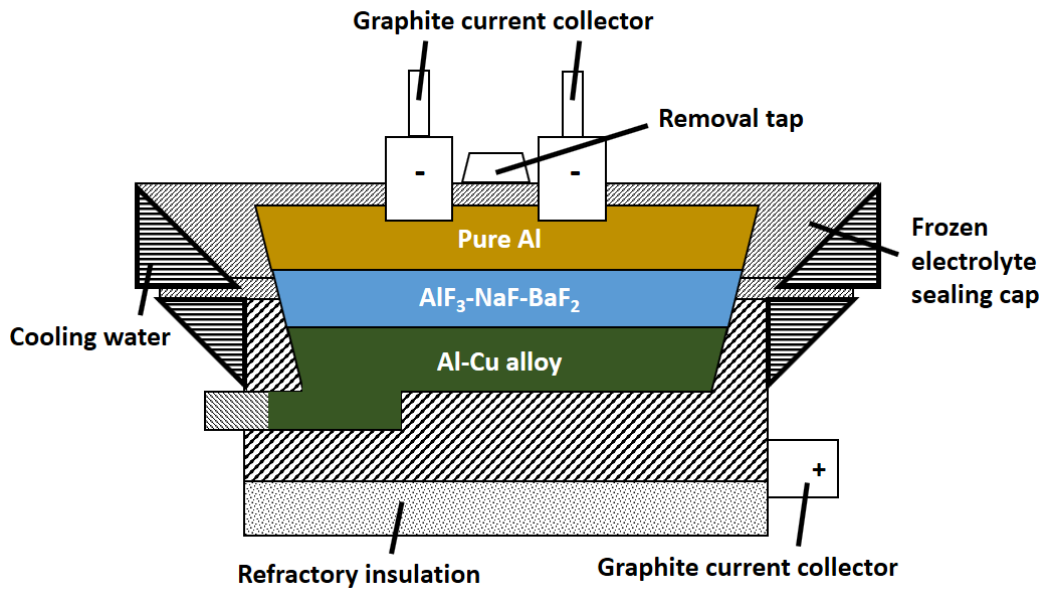
Figure 5. Schematic of a Hoopes cell composed of three-liquid-layer for production of pure aluminum through electrochemical charge.[25]
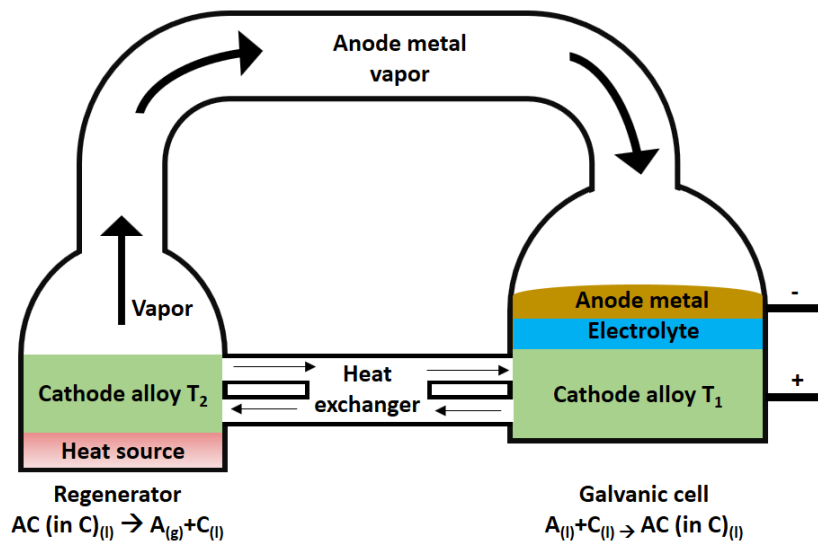
Figure 6. Schematic of thermally regenerative bimetallic cell composed of regenerator part and galvanic cell part depicted by Argonne National Laboratory.[26]
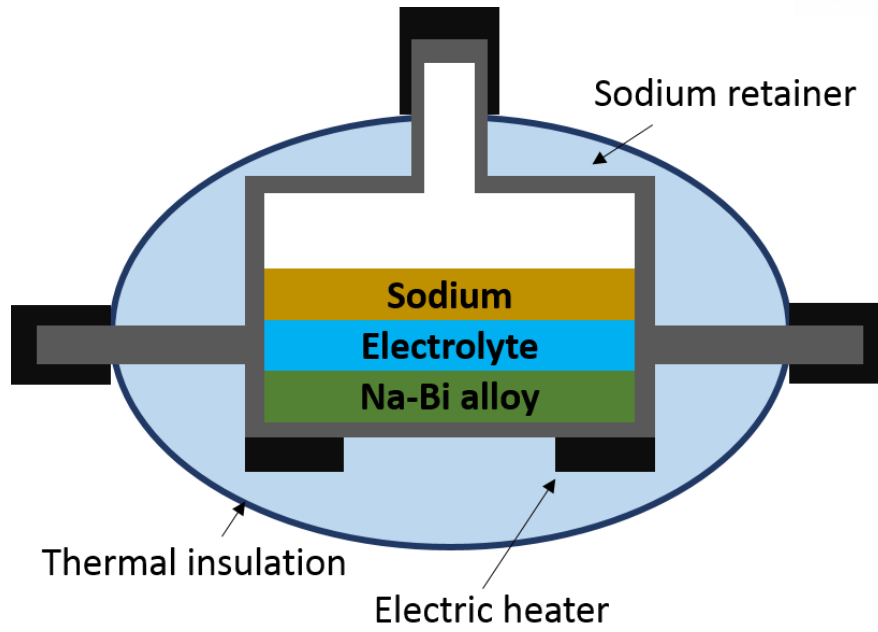
Figure 7. Schematic of bimetallic secondary cell composed of Na|NaF-NaCl-NaI|Bi depicted

by Argonne National Laboratory.[27]

1.3.2. Research background

LMBs are composed of anode, cathode, and electrolyte equally to other batteries, however, those are all-liquid state during an operation. Those self-segregate into unmixed distinct three layer by their density and immiscibility. The top of three layers is anode, middle of that is naturally electrolyte, which is electrical insulator as broadening the gap between anode and cathode, and bottom of that is cathode as shown in Figure 8. During discharge, the negative electrode, liquid metal A is electrochemically oxidized($A \rightarrow A^{z+} + ze^-$) and then it migrates to the positive electrode, liquid metal B, through the electrolyte. Finally, liquid metal A-B alloy will be formed (A in B), while releasing electrons into an external circuit. The reverse reactions occur upon charging $(A^{z+} + ze^- \rightarrow A)$.[5] In accordance with the Nernst equation, the difference in the chemical potentials of pure liquid metal A and liquid metal A in liquid metal B can determine a cell voltage in the following equation,

$$E_{cell} = \frac{RT}{nF} \ln[\frac{a_{A(inB)}}{a_A}]$$

Where R is the gas constant, T is operating temperature in Kelvins, F is the Faraday constant, a_A is the activity of pure A, $a_{A(inB)}$ is the activity of A in B.

Candidates of anode and cathode materials are required to satisfy the following issues.[27]

(1) Melting temperature of materials should be lower than 1000 ºC and the boiling point higher than 25 ºC.

(2) Minimum electronic conductivity higher than the ionic conductivity of a molten salt electrolyte (σ > 1 S cm⁻¹).

(3) Nonradioactive and stable isotope.

Candidates materials, which are following above requirements, are marked in periodic table as shown in Figure 9. Alkali and alkaline-earth metal have low density and electropositive materials enough to be anode. Actinides and heavy metal marked in periodic table have high

density and electronegative materials enough to be cathode. In Figure 10, those are also divided into negative and positive electrode materials by reduction potential compared with standard hydrogen electrode (SHE) in aqueous solutions.[28] If those have lower potential than -2.0 V, those are used for negative electrode. If those have higher potential than -1.0 V, those are used for positive electrode.
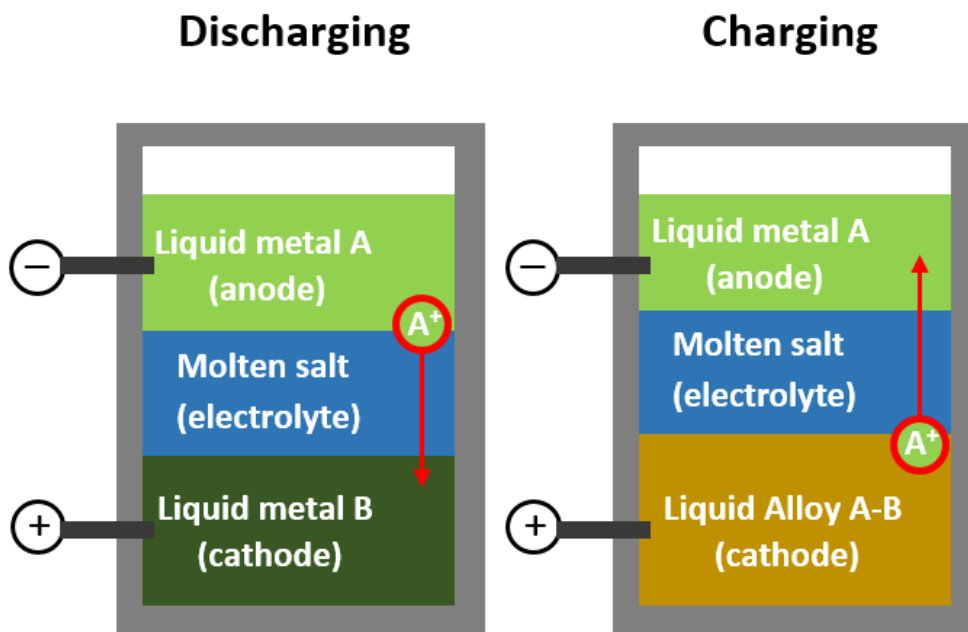
Figure 8. Schematic diagram of liquid metal batteries on charge and discharge.

Figure 9. Candidates materials of anode(yellow) and cathode(green) in periodic table.[27]
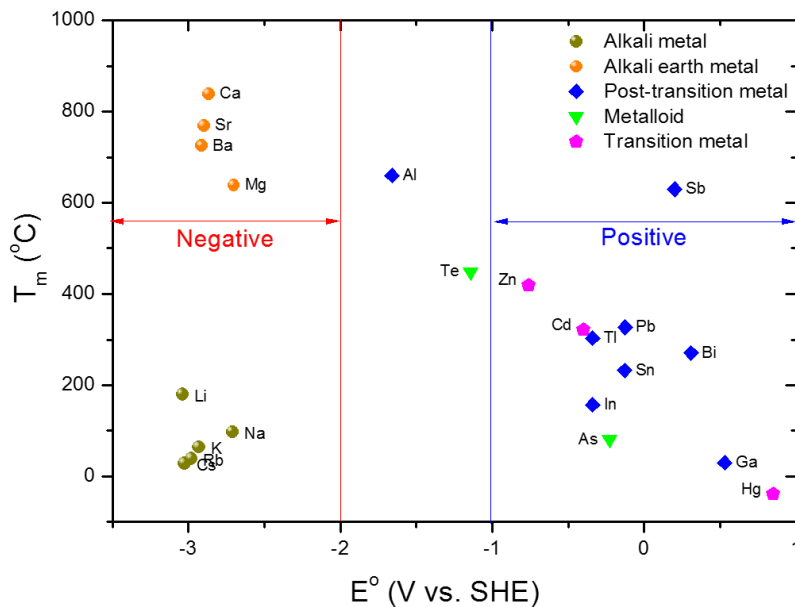
Figure 10. Marked points those are candidates materials of negative and positive electrode according to their deposition potentials (vs SHE) in aqueous solutions and their melting temperature.[28]

To select suitable molten salt as electrolyte, the following requirements are significantly considered. Firstly, it should have intermediate density compared with anode and cathode. If this requirement isn't satisfied, they interosculate and then, finally, a short circuit will occur. Secondly, it is preferred that the melting temperature is similar to operating temperature. If operating temperature is much higher than the melting temperature, molten salt will be exhausted. Material loss could influence on influencing to efficiency. Thirdly, if its metal solubility has lower values, the self-discharge becomes smaller. In LMBs, the self-discharge means that anode material melt in molten salt. The reason of its cause has not exactly been revealed but several speculated mechanisms have been suggested.[27, 29, 34] as mentioned above, candidates of anode materials are alkali and alkaline-earth metals. Molten salt electrolyte has ionized metals to move to cathode such as LiCl, LiI, NaCl, $MgCl_2$, etc. Solubility of anode materials in halide salts comes out into the open quantitatively through a precedent study as shown in Table 1.[27, 30, 31, 32] Therefore, when choosing salt, solubility of that is surely considered.

Table 1. Solubility of lithium and sodium metals in their halide salts at certain temperature.[30, 31, 32, 55]

Salt	Solubility (mol %)	Temperature (°C)
LiF	1.0	847
LiCl	0.5-2.0	640-1000
LiI	1.0-2.5	468-950
NaF	3.0	990
NaCl	2.1	795
NaBr	2.9	740
NaI	1.6	657

1.4. Research proposal

1.4.1. Objective of study

Most of the researchers have easily used purchased customized cell such as coin type cell for testing electrochemical properties of their synthesized materials due to formerly developed standard cells for conventional batteries. Without these optimized standard cell, they possibly have difficulty from analysis of results because of many variables. Therefore, using standard cell, it is relatively easy to analyze results and compare them with each other. In LMBs, optimized standard cell development is helpful to researchers who want to study LMBs because there is no clearly recognized standard cell. In my thesis, the ways of setting up standard cells and results such as electrochemical performance are introduced.

1.4.2. Design and fabrication process for standard cell

As shown in Figure 11, in the first step, the first cell is designed for electrochemical test. A vessel, which embraces cell, and furnace for heating up cell are also contrived. The next step is fabricating all designed components and then to confirm whether a fabricated cell is optimized or not through electrochemical performance of selected materials. If problems are detected on designed cell through measured results data and post mortem, the first cell should be modified to the second cell. Evaluating, analyzing, and improving steps are repeated until electrochemical performances are stabilized.
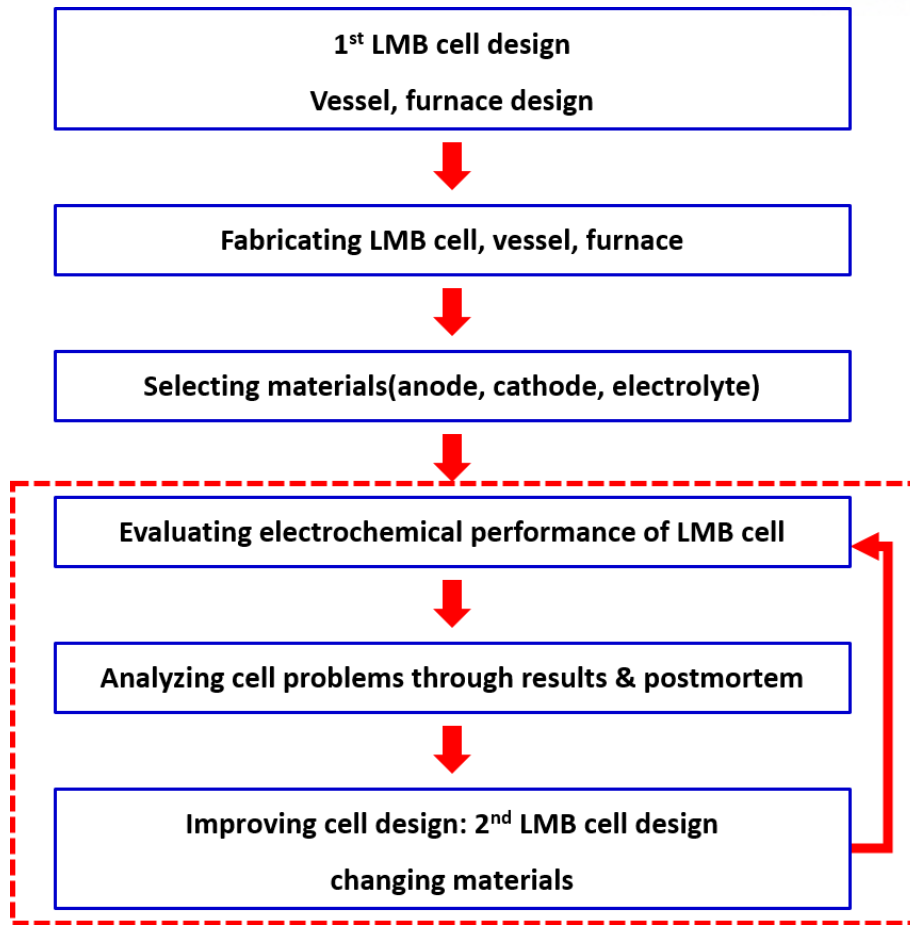
Figure 11. Flow chart of ways of standard cell set up composed of six steps, red line marked three steps is repeated.

1.4.3. Electrochemical measurement and characterization

Galvanostatic method, which is constant current is applied to electrochemical cell using cycler (WBCS 3000, Wonatech), was used for analyzing voltage profile during charge and discharge reaction, additionally, possibility of long-term cycle was examined. Internal resistance and reversible redox reaction were qualitatively measured by cyclic voltammetry (ZIVE SP2, Wonatech). Through this method, mass and charge transfer were also qualitatively analyzed. Ohmic resistance and charge transfer resistance were measured by electrochemical impedance spectroscopy (ZIVE SP2, Wonatech). Measuring extent of self-discharge is quite important in practical batteries. As previously mentioned, in case of LMB, using molten salt as electrolyte with liquid electrode, its solubility generates self-discharge. Leakage current, which means degree of self-discharge, was quantitatively measured using stepped-potential measurement (ZIVE SP2, Wonatech). Stepped-potential measurement is that voltage is applied above OCV for period of time and then saturation current is measured after applying higher voltage than before.

In previously reported paper, characterization has been reported using X-ray diffraction (XRD), Scanning electron microscope (SEM), Energy dispersive spectrometry (EDS) of inner materials after cross section by cutting in half. In this study, these characterization is very hardly translated into action because of technical difficulties about cell cross section. Because LMBs include alkali, alkali-earth metal, those are instability with air, especially, water, as anode materials. Therefore, cutting facility using water is not suitable for these case, instead optically investigation such as postmortem came into action as opening cell cap. Additionally, practical study was carried out, so called cool down test. It will be explained in section 4.3. Molten salt was analyzed by thermogravimetric analysis (TGA, Q600 SDT) and differential scanning calorimetry (DSC, Q600 SDT) to confirm melting point of that through heat flow.

2. Chapter 1. First design of LMB cell

2.1. Design and choice of cell components

First cell was designed and fabricated as mentioned ways of cell setting up. Basic cell components are composed of positive current collector, negative current collector, and insulator except for anode, cathode, and electrolyte as shown in Figure 12. Material for positive current collector should have electrical conductivity and, also, act as a container for anode, cathode, and electrolyte. Additionally, considering the operating temperature of LMBs, positive current collector devoid of degradation, which is originated from high temperature and side reaction with inner material, should be designed. Precedent research of mutual interaction between positive current collector, which uses steel and stainless steel, and Sb-Pb alloy are reported.[33] Cell based on stainless steel forms stable intermetallic compounds at constant temperature (450 °C) under Ar atmosphere for 500 hours. SUS304, which consists of iron as base material and 18~20 % of it is nickel, is widely known as having outstanding corrosion resistance in general corrosion environment except for chlorine. Therefore, SUS304 is selected for starting material of positive current collector and, also, negative current collector. Insulator is used for preventing cell short caused by direct contact between positive current collector and negative current collector. Considering LMBs operated at high temperature, more than 400 °C, it should endure that temperature. Ceramic materials are generally served as insulator and they withstand high melting temperature (1000-1600 °C). Therefore, alumina (Al_2O_3) is selected as insulator of cell because of relatively low cost and it is generally used.

Outward form of the cell was designed based on autoclave developed by Charles Chamberland in 1879. The autoclave has been mostly used for sterilization at a high temperature, with applications to a wide range of field such as biology, medicine, material engineering, etc. Especially, hydrothermal synthesis has been widely used to synthesize

nanomaterials such as metal oxide particles using hydrothermal autoclave as shown in Figure 13.[35, 36, 37, 38] To endure high pressure due to higher operating temperature than melting or boiling point of water or organic solvent, it uses compressive sealing with thread. In LMBs, although operating temperature is higher than melting point of inner materials such as anode, cathode, and electrolyte, it is highly lower than the boiling point of that. Therefore, applying autoclave to LMB cell design seems to experimentally be safer than using that of nanomaterial synthesis. In Figure 14, blueprints and manufactured of the cell are shown. It is composed of cell cup, in which inner materials are inserted, and cap as well as those are combined by the usage of thread. Concretely, hole is manufactured for inserting negative current collector bar. To easily connect to the electrochemical measurement facility, the negative current collector was designed as shape of bar and to smoothly contact with anode material. Its tip was shaved regularly as shown in Figure 15. Positive current collector was also manufactured as shape of a bar.
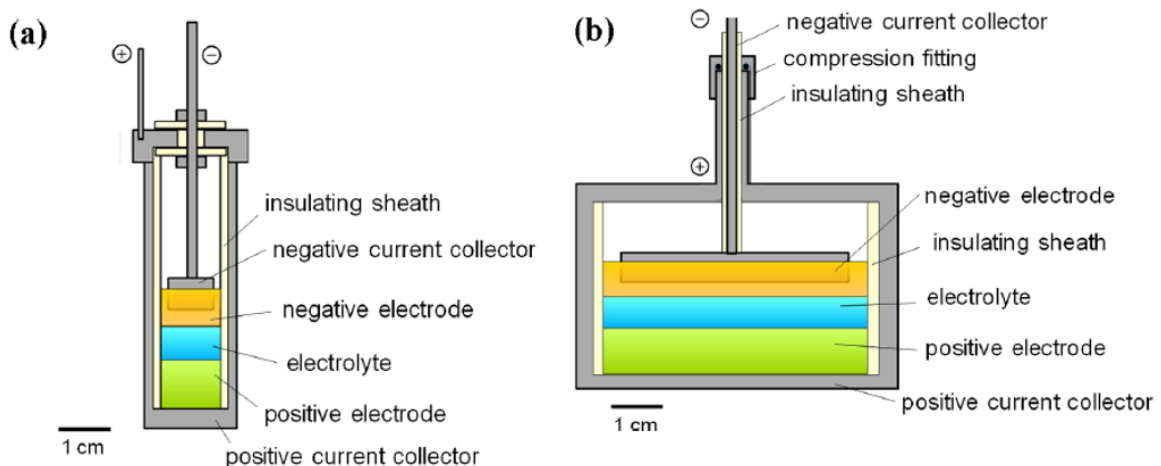
Figure 12. Illustration of cell structures of liquid metal batteries. (a) unsealed small type cell and (b) sealed cell using compression fitting.[24]

Figure 13. Assembled hydrothermal autoclave and their components such as cup, cap, and plastic(Teflon) crucible manufactured by Zhengzhou Keda Machinery and Instrument Equipment Co., Ltd.
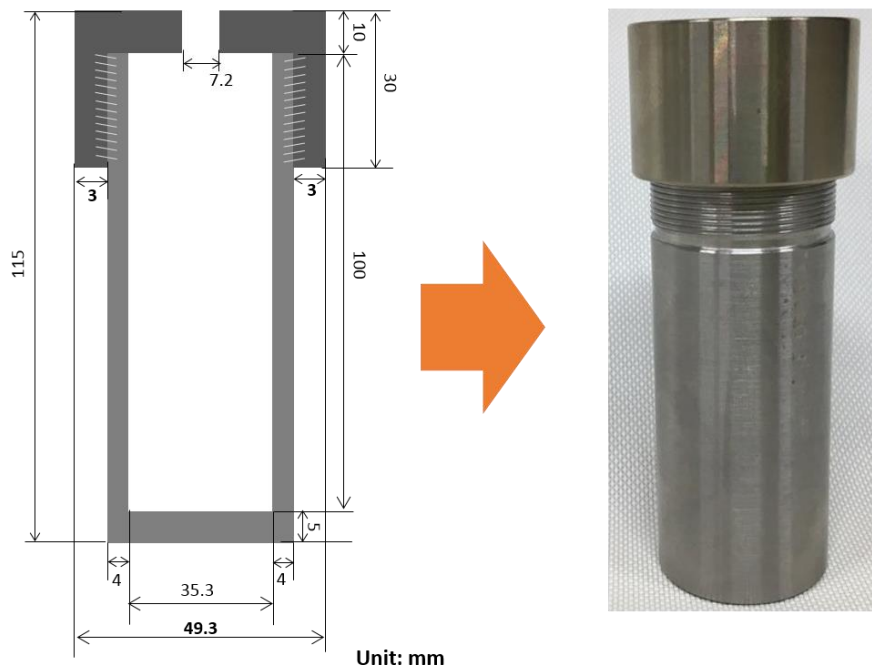
Figure 14. Design map of cell cap and cup as positive current collector and fabricated theirs.
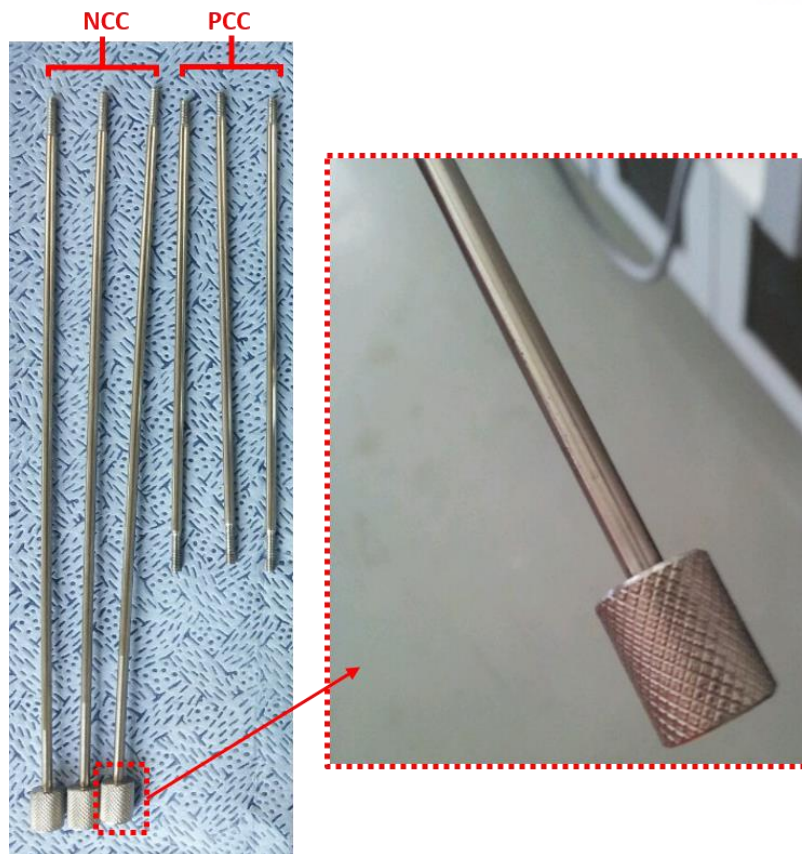
Figure 15. Fabricated bar type negative current collector, which has shaved tip, and positive current collector.

Al$_2$O$_3$ tube was used for insulating between positive and negative current collector. Adhesive and sealant is required because using only Al$_2$O$_3$ tube is not enough to protect inflow of exterior atmosphere and hold on a negative current collector. In this case, previous research about solid oxide fuel cells (SOFCs) reported that glass-ceramic or ceramic sealant has been used for sealing.[39, 40, 41] Considering the operating temperature (800~1000 °C) of SOFCs is relatively higher than that (200~500 °C) of LMBs, these sealants are evaluated as suitable for LMBs. Sealants consist of particles of SrO, La$_2$O$_3$, Al$_2$O$_3$, B$_2$O$_3$, SiO$_2$, etc and organic solvent.

After curing process, solvent will be vaporized and then particles will stiffen for sealing. These have outstanding adhesive strength to other materials such as metal, plastic. Ceramic sealant (Ceramabond 552-VGF, Aremco Products Inc.), which has superior adhesive strength with ceramic and metal, was selected.

Using designed cell, electrochemical properties of inner material were evaluated using solid electrolyte. Purpose of that was excluding unexpected risk and explosion due to the first attempt of high temperature batteries and unwanted reaction such as mix of anode and cathode. Sodium-sulfur (NaS) batteries and Zero-emission batteries research activities (ZEBRA), widely known as using solid electrolyte, have used Na, β"-Al_2O_3 (Ionotec Ltd). It was selected as electrolyte for first designed LMB cell, naturally, sodium was selected as anode material.[10, 16] Ionic conductivity and ionic diffusion, those directly affect electrochemical performance, are examined through precedent study.[42, 43, 44] As show in Figure 16, Na, β"-Al_2O_3 of cup type was used to put Na inside it. In Table 2, candidates of cathode materials, those are reacted with sodium as alloying, are shown. Mercury (Hg), tin (Sn), and bismuth (Bi) have melting point under 300 ℃ but, considering environmental pollution and biohazardous, Hg is not suitable for cathode. Sn was selected as cathode of Na anode because it has relatively lower cost and melting point ($T_{m\ of\ Sn}$=231.93 ℃, $T_{m\ of\ Bi}$=271.5 ℃) than Bi. Sequence of cell assembly is shown in Figure 17. Cell cap, which acts as positive current collector, were insulated with negative current collector due to Al_2O_3 tube and then it was fixed using ceramic sealant by the following process.

Curing process: Drying in air, 4 h → Heating in furnace, 3 h @ 80 ℃ → Heating in furnace, 3 h @ 260 ℃

After curing, the cell cap was moved into glove box filled with argon (Ar) gas and then Na metal (ACS reagent, Sigma-Aldrich) was attached at negative current collector tip. In cell cup, Na, β''-Al$_2$O$_3$ was inserted and then Sn powder (99.8 %, Sigma-Aldrich) was injected between inner wall of cell cup and Na, β''-Al$_2$O$_3$. Finally, the cell cap with Na metal was combined with the cell cup carefully.
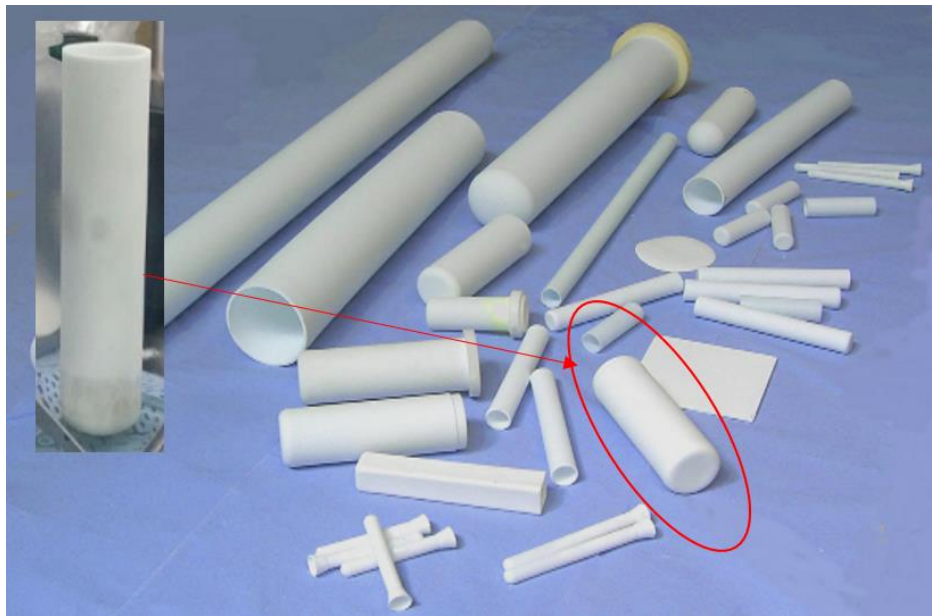
Figure 16. Cup type commercialized Na, β''-Al$_2$O$_3$ manufactured by Ionotec Ltd.

Cathode	$E_{cell,eq}$ [V]	T_m [°C]	P_i [$/mol]
Zn	-	420	0.15
Cd	0.12	321	0.39
Hg	0.40	-39	0.27
Al	-	660	0.066
Sn	0.34	232	3.2
Pb	0.34	327	0.52
Sb	0.74	631	1.8
Bi	0.61	271	4.9

Table 2. Equilibrium cell voltage (versus Na^+/Na), melting temperature, and cost of candidates cathode materials.[26]
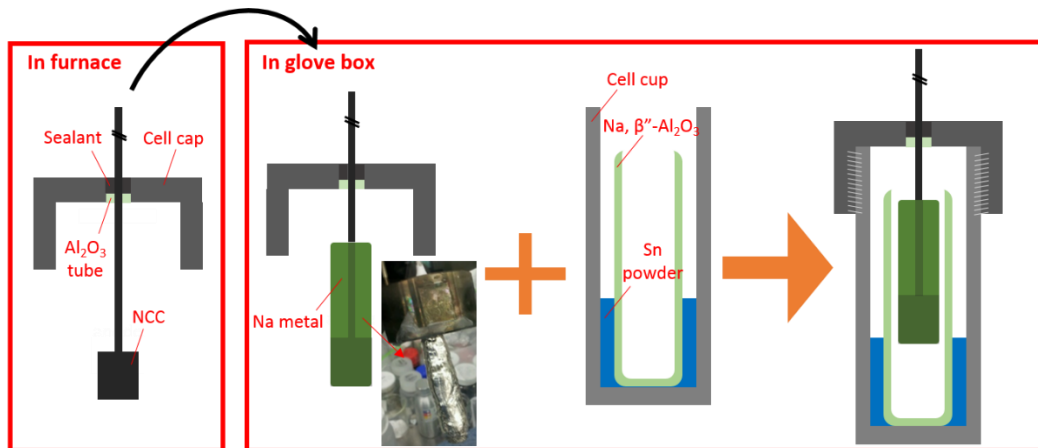
Figure 17. Assembly process of Na| Na, β''-Al$_2$O$_3$|Sn liquid metal battery cell in furnace and glove box.

Assembled cell had to be operated in furnace because inner materials such as anode, cathode, and electrolyte should be liquid state. Therefore, customized vessel and furnace were fabricated. Assembled was inserted into customized vessel, which consist of quartz cup and aluminum cap, and then it was combined with customized furnace as shown in Figure 18. Possibility of reaction between Na and atmosphere is probably existed due to unstable sealing using thread. To avoid that, Ar gas was used for making inert atmosphere around cell, therefore, gas inlet and outlet was manufactured on aluminum cap. Pictures of manufactured customized vessel and furnace are shown in Figure 19.
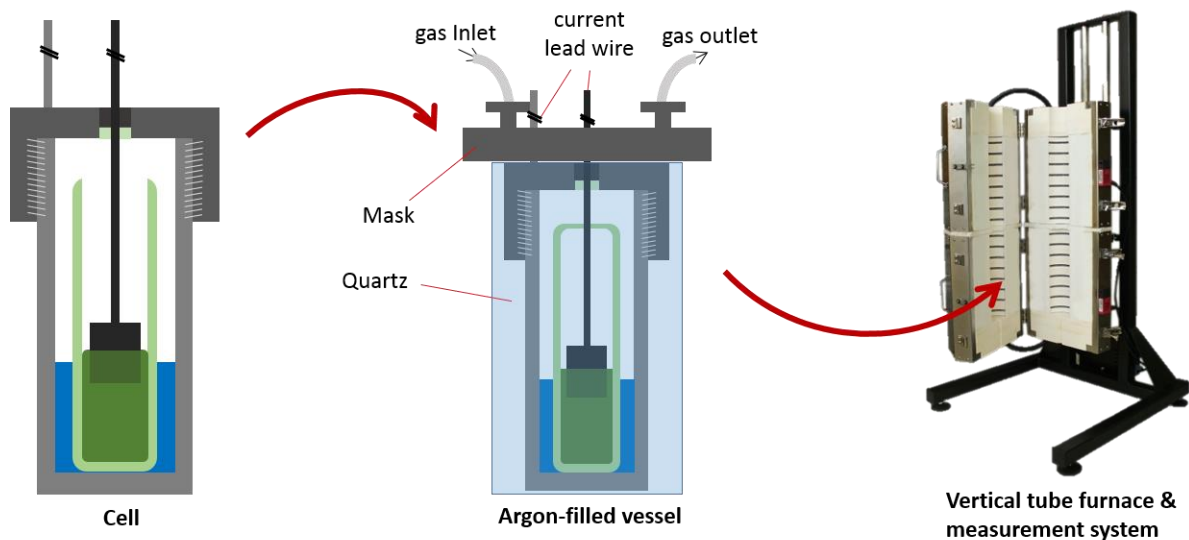
Figure 18. Process and design of Ar gas flowing system. In first step, insertion of cell into vessel compsed of mask and quartz tube. In second step, insertion combined cell and vessel into vertical tube furnace.
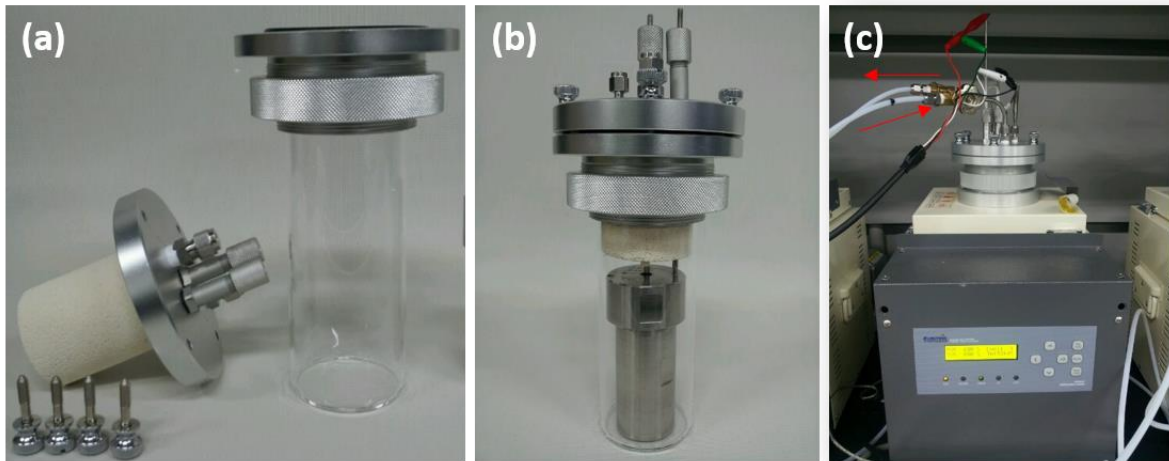
Figure 19. Fabricated vessel and measurement system. (a) furnace mask and quartz tube, (b) assembled cell in a vessel, and (c) customized furnace equipped with vessel.

2.2. Electrochemical performances of Na| Na, β"-Al$_2$O$_3$|Sn cell

When operating temperature of Na||Sn is set at 300 ℃, liquid Na is inserted into liquid Sn following red line as shown in Na-Sn phase diagram in Figure 20. On the Na-Sn phase diagram, liquid state of cathode is maintained until inserting 20 mol% of liquid Na into liquid Sn. In case it is above that value, Na$_7$Sn$_{12}$ solid phase will presumably be emerged. When applying the current of 1 mA during 30 minutes both charge and discharge, those were smoothly proceeded as shown in Figure 21(a) and the change of voltage profile appeared while cycling were proceeded as shown in Figure 21(b). There were many trials and errors in trying to get a smooth performance (more detail in appendix A). Plateau of discharge voltage was built at 0.75 V and 2 V during the cycling. The charge of voltage was built at 2.29 V and it became more stabilized at 2.29 V during the cycling. During discharge, overpotential was raised due to resistance of

charge and mass transfer caused by insertion liquid Na into liquid Sn through Na, β"-Al_2O_3.

According to Gibbs phase rule, plateau of discharge voltage is originated from Na-Sn liquid

and Na_7Sn_{12} solid phase but contrary to expectations, solid phase is generated before insertion

20 mol% of liquid Na into liquid Sn. Partial mole concentration of liquid Na between Na, β"-

Al_2O_3 and liquid Sn exceeded above 20 mol%, therefore, as shown in Figure 22, solid phase

(brown line) is formed.

There are failures due to using Na, β"-Al_2O_3. When applying 20 mA to Na||Sn cell, it was

broken as shown in Figure 23 of postmortem. This is because it didn't endure high current

applied to small contact area between liquid Na and it.[45] In addition, Na which was contained

in it was almost exhausted after postmortem probably because of vaporization of liquid Na at

operating temperature.
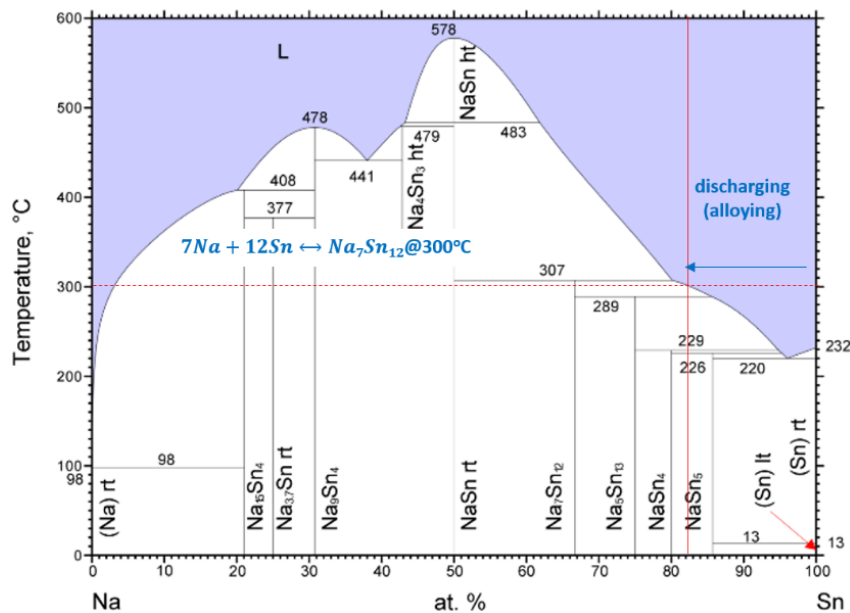
Figure 20. Na-Sn phase diagram. The alloying reaction at 300 ℃ (red line).
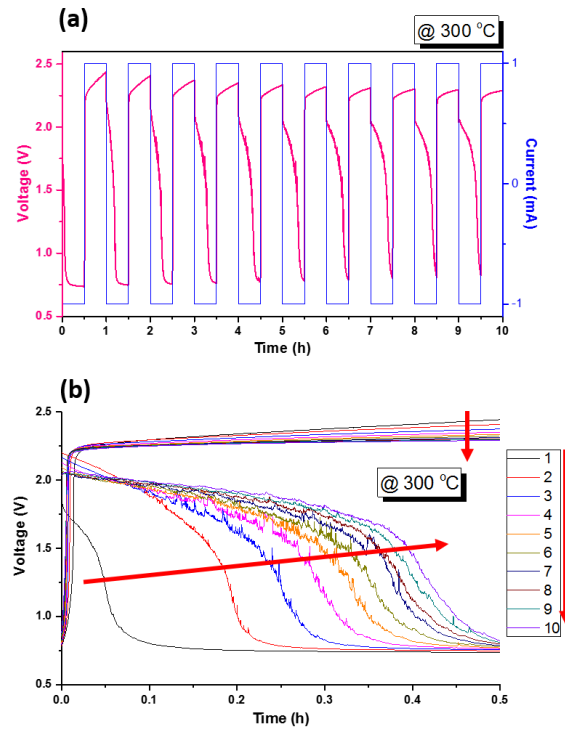
Figure 21. Electrochemical performance of Na| Na, β"-Al₂O₃ |Sn LMB cell. Galanostatic charge-discharge cycling at 1 mA, 300 °C. (a) Voltage profiles in accordance with respect to time and (b) step time.
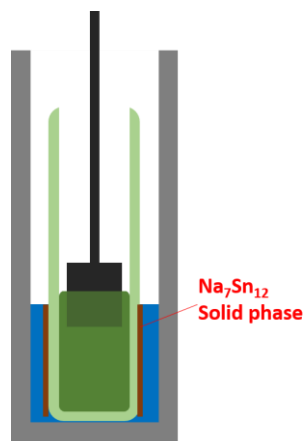
Figure 22. Na₇Sn₁₂ solid phase (brown line) between Na, β"-Al₂O₃ and liquid Sn through expactated cross section of Na||Sn cell.
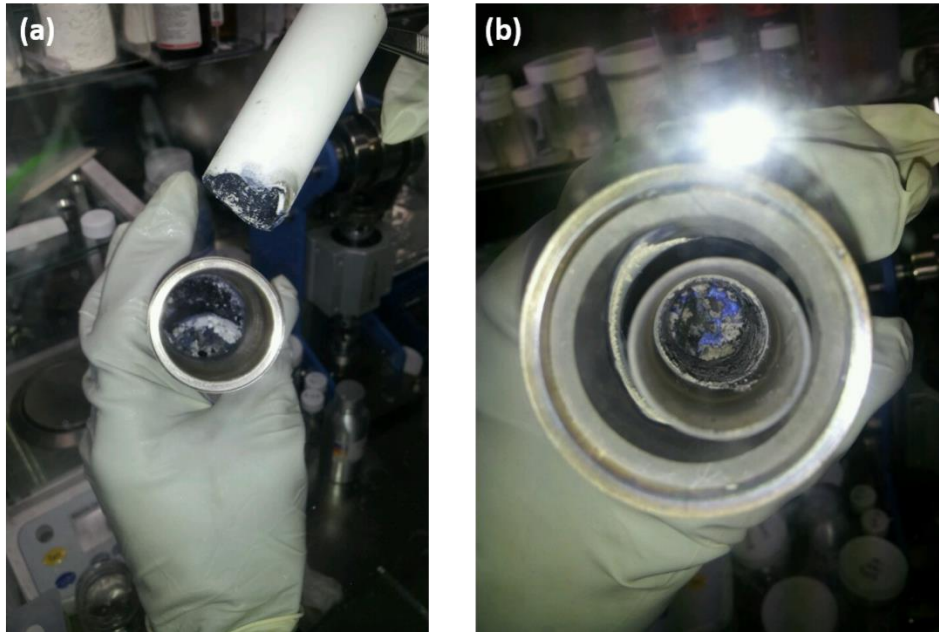
Figure 23. Post mortem image of Na||Sn cell (a) after 20 mA applied and of (b) exhausted Na in Na, Na, β''-Al$_2$O$_3$.

2.3. Summary

Through first cell design, basic cell structure and measurement system were fabricated. Using these manufacture things, electrochemical performance of Na|Na, β"-Al$_2$O$_3$|Sn cell was measured and analyzed. Intended goal, which is grasping possibility of the operation of designed cell through galvanostatic measurement, was accomplished. To solve the mentioned problems, modifying cell design and selecting material passed off.

3. Chapter 2. Second design of LMBs cell

3.1. Design and choice of cell components

In the second design, basic cell structure was not changed, but inner materials were changed or added. The Na, β"-Al$_2$O$_3$ was removed to avoid high polarization and demonstrate three-liquid-layer LMB cell using molten salt as electrolyte. Referring to a previous research paper, magnesium (Mg, T$_m$= 650 °C) as anode, MgCl$_2$-NaCl-KCl (50:30:20 mol%, T$_m$= 396 °C) as electrolyte, antimony (Sb, T$_m$= 630 °C), and graphite crucible, which is not reacted with Sb, as positive current collector were used.[24] Molten salt electrolyte was prepared as follows,

(1) MgCl$_2$ (99%, Alfa aesar), NaCl (99%, Alfa aesar), and KCl (>99%, Sigma-Aldrich) are mixed at the rate of 50:30:20 mol%

(2) Put mixed salt into graphite crucible and then insert that into cell cup

(3) Cell cup and cell cap, which don't have a hole, are combined and then heat up to 600 °C for 15 hours in Ar gas flowing furnace

(4) Put pre-melted salt on it and then grind it using a mortar

Al$_2$O$_3$ tube was used as insulator for avoiding directly contact between Mg and graphite crucible. In Figure 24(a), expected cross section of assembled Mg|MgCl$_2$-NaCl-KCl|Sb cell is described and experimental pictures, those are insertion graphite crucible and Al$_2$O$_3$ tube into cell cup, were shown in Figure 24(b). Those were cleaned using ethyl alcohol and D.I water. The process, which is that attaching negative current collector to cell cap, is same the as first cell. Those were inserted into cell cup in order and then, also, Sb, salt, and cell cap were added and combined during assembly process. Finally, assembled cell was inserted into furnace under Ar gas flowing.
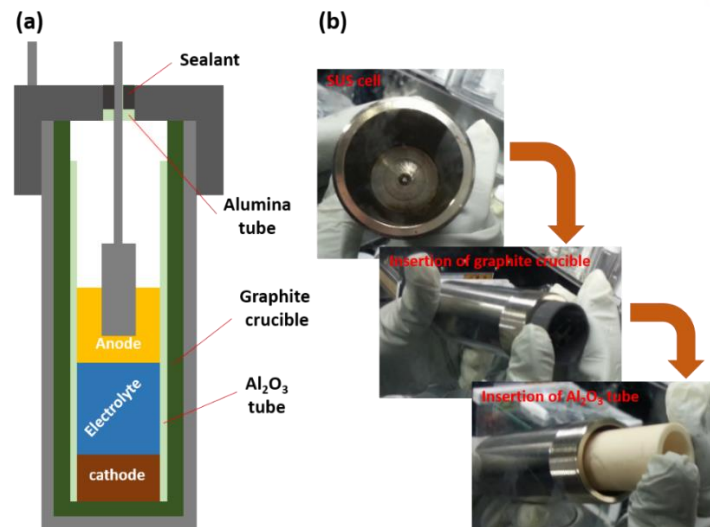
Figure 24. Second designed LMB cell. (a) schematic drawing the cross-sectional view of the cell and (b) assembly process showing graphite crucible and insulating Al₂O₃ tube.

3.2. Electrochemical performances of Mg|MgCl₂-NaCl-KCl|Sb cell

In Figure 25(a), the change of OCV is shown while it was heated up to 680 °C as operating temperature and it was saturated at about 0.53 V. The result of 20 mA and 50 mA galvanostatic performance is shown in Figure 25(b). When applying the current of 50 mA, charge and discharge smoothly proceeded for 10 hours each, although the cell short occurred in the 6th cycle. Before occurrence of cell short, in charge in the 5th cycle, voltage profile was an uncommon shape. It means that the unknown factors made these results. In addition, these electrochemical performances were obtained after several tries and errors (more detail in appendix B).

Direct contact between anode and cathode or external circuits, which are positive current collector and negative current collector, are required for cell short. To examine the inside of the cell, after reducing temperature, cell cap was opened and the picture of the inside is shown in Figure 26. When opening the cell cap, it was easy because the negative current collector tip (Figure 26(a)) was not fully immersed in liquid Mg or molten salt electrolyte. As shown in Figure 26(b), Mg was not placed on an exact top position, but it looks like a little sink in salt. In Figure 27, the expected cross section of Mg||Sb at operating temperature, most of liquid Mg is placed into molten salt electrolyte and a small quantity of that sticks out differently in Figure 24. Density of liquid Mg is 1.6 g cm⁻³ and in previously research paper, that of NaCl, KCl, and MgCl₂ are 1.8, 1.6, and 1.75 g cm⁻³ respectively.[46] Above 600 °C, that of electrolyte is almost no difference with liquid Mg. Additionally, as shown in Figure 28, the higher temperature results in lower density of MgCl₂-NaCl through change of density along the temperature.[47] As a result, liquid Mg probably sank into electrolyte or not exactly separated with that because of their density, therefore, those induced cell shorts. As shown in Figure 29, through Ellingham's diagram and change of Gibbs free energy, aluminum (Al) and magnesia (MgO) are generated

due to reaction between Mg and Al_2O_3. After several cycling, anodes would sink due to higher density of Al (2.38 g cm^{-3}) than that of Mg. Therefore, Al_2O_3 as insulator is not suitable in Mg|$MgCl_2$-NaCl-KCl|Sb cell.[48]

When using Al_2O_3 tube in liquid Na anode LMB cell, it is stable. Therefore, Na (T_m= 98 ℃) as anode, NaOH-NaI (80:20 mol%, T_m= 220 ℃) as electrolyte, and Bi-Pb (56:44 mol%, T_m= 125 ℃) were selected referring previous research.[49] As mentioned in section 2.3, liquid Na vaporization is must considered on high operating temperature. However, that could be alleviated as operating at lower temperature using materials that have low melting temperature. In next section, LBM cell using Na as anode will be explained.
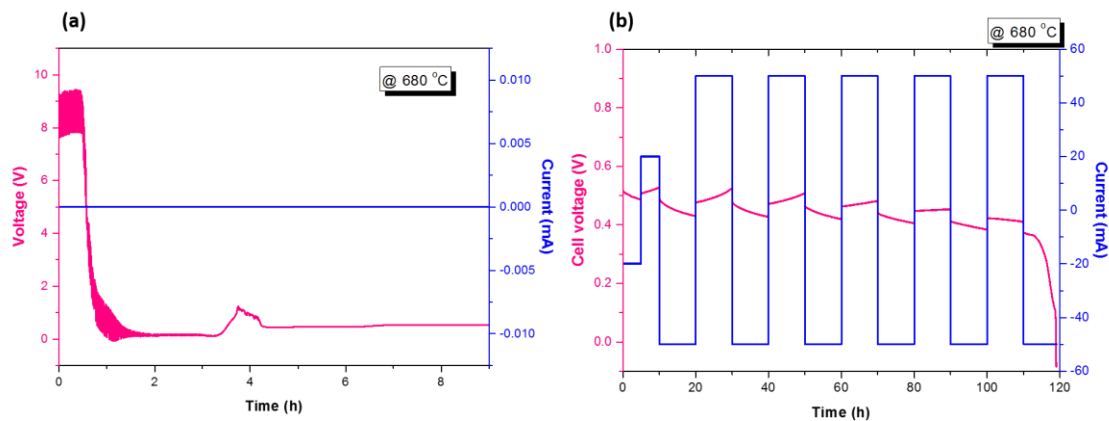
Figure 25. Electrochemical testing of Mg|$MgCl_2$-NaCl-KCl|Sb LMB cell at 680 ℃. (a) Variation of open circuit voltage (OCV) during heat up and (b) galvanostatic cycling at 20 mA and 50 mA.
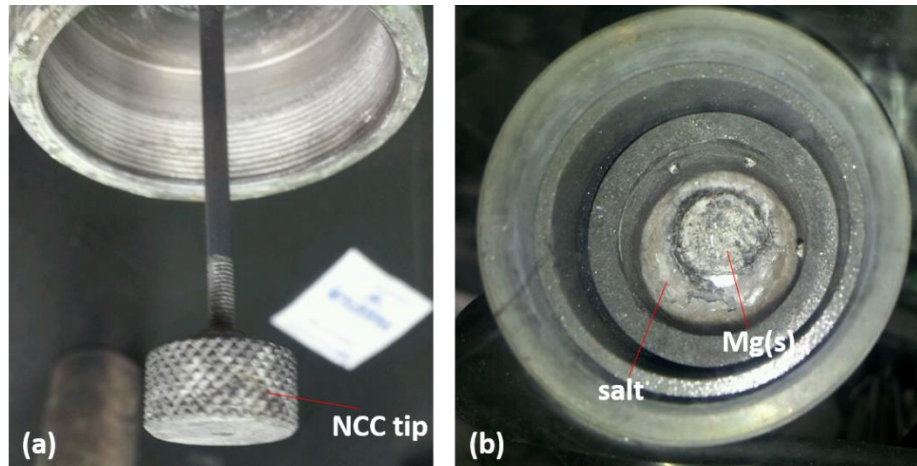
Figure 26. Post mortem images of Mg|MgCl$_2$-NaCl-KCl|Sb. (a) Image of negative current collector tip and (b) inside materials such as Mg, salt, graphite crucible, and insulator.
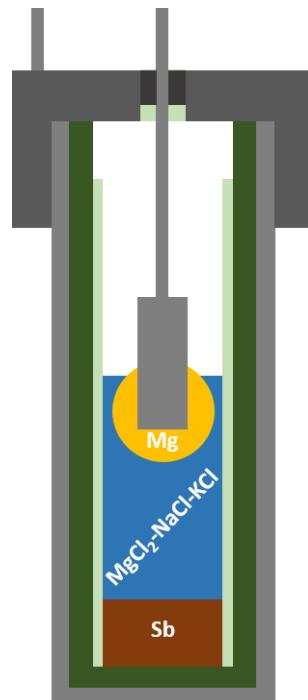
Figure 27. Expected cross section of Mg|MgCl$_2$-NaCl-KCl|Sb at operated condition. Sinked Mg into MgCl$_2$-NaCl-KCl.
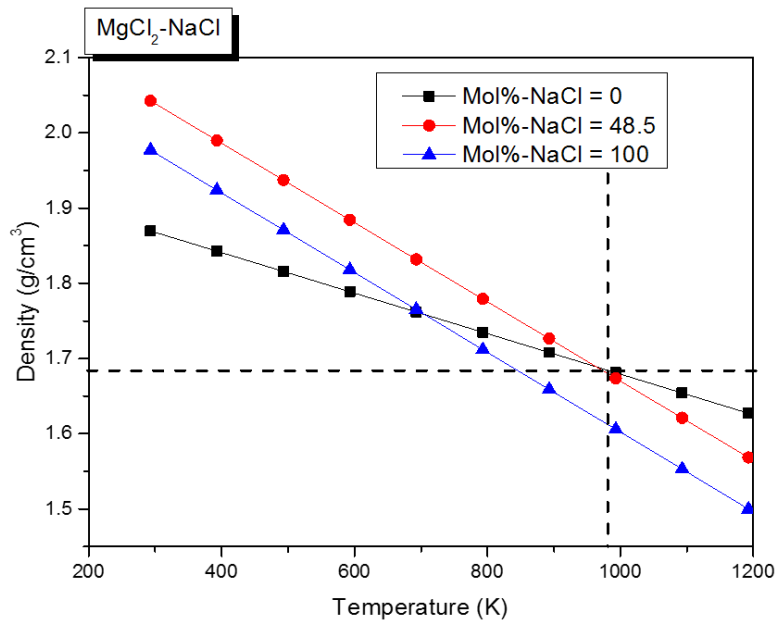
Figure 28. Variation in density of MgCl$_2$-NaCl in various compositions according to temperature.

$$3Mg + Al_2O_3 \rightarrow 2Al + 3MgO$$

$$\Delta_r G = -118 \ kJ/mol \ at \ 727 \ ^oC$$
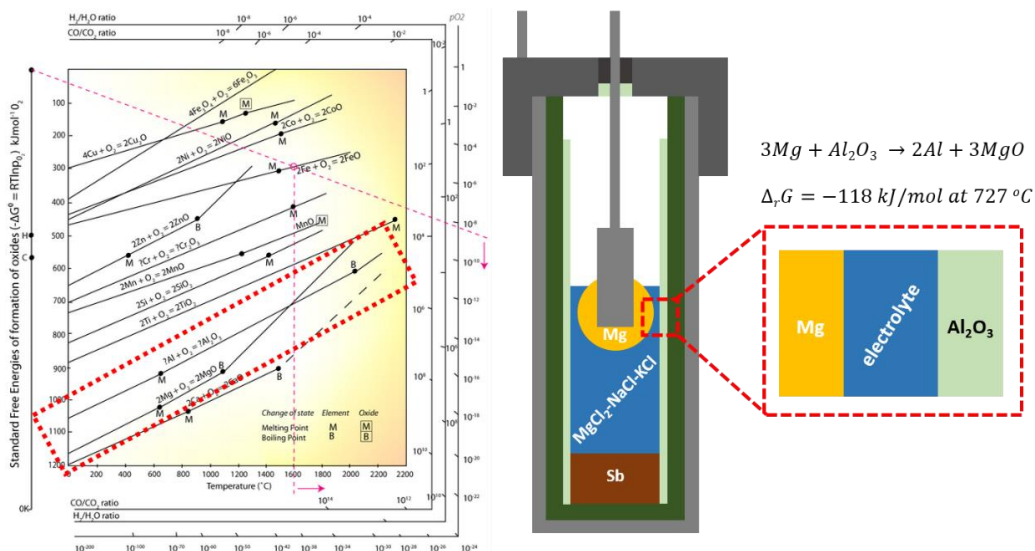
Figure 29. Ellingham diamgram and shematic of expected thermadynamically spotaneous side reation between Mg and Al$_2$O$_3$ tube.

3.3. Fabrication and electrochemical performances of Na|NaOH-NaI|Bi-Pb cell

Na metal was attached to negative current collector in Figure 17. It was prepared with the same process, but negative current collector tip was combined with negative current collector using thread and nut as shown in Figure 30. NaOH-NaI salt was made using cell cap without hole, cell cup, and graphite crucible as shown in Figure 31(a). NaI power (T_m= 661 °C) was placed in the bottom and NaOH powder (T_m= 328 °C) covered NaI as placing top position. This is because NaI is highly volatile at nearly melting temperature, therefore, NaOH is homogeneously mixed with NaI while NaOH is melting earlier than NaI. Heat-treatment sequences are as follows during the manufacture process.

Temperature sequences: 150 °C, 2h → 250 °C, 2h → 350 °C, 4h → 550 °C, 6h → 200 °C, 4h → room temperature

Each step has purpose that surface water, organic impurities, and inner moisture are eliminated from the first to the third step. From the third to the fourth step, the NaOH is melted and sinks into NaI powder. In the fifth step, homogeneous phase is formed as slowly decreasing temperature.[49] Manufactured salt was grinded as shown in Figure 31(b) and after that, TGA and DSC are measured to confirm the melting temperature of manufactured salt as shown in Figure 32. Endothermic reaction was raised at 220.16 °C nearly equal to the reported data, so therefore, it was manufactured with a targeted composition. Bi-Pb of eutectic composition alloy was manufacture by mixing bulk Bi (99.997 %, Alfa aesar) and Pb (99.999 %, Alfa aeasar). After that, the cell assembly process was equal to Mg||Sb LMB cell.
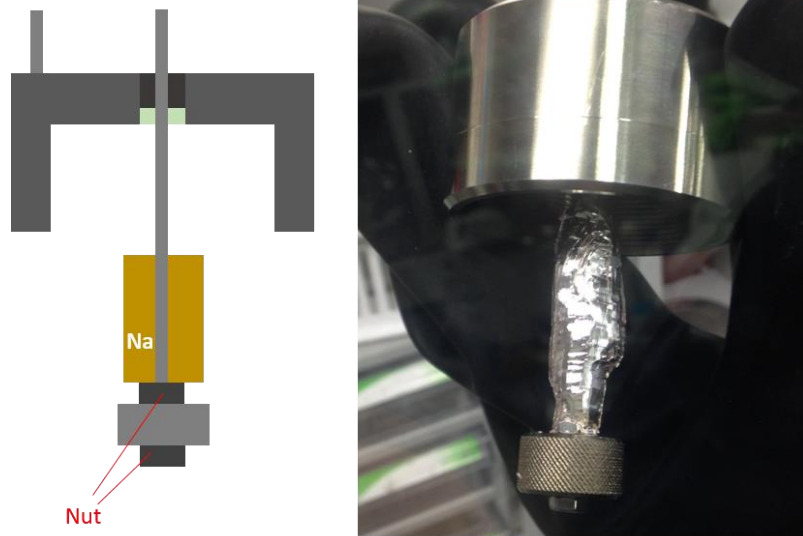
Figure 30. Cross section of assemble cell cap (cell cap+Negative current collector+Na metal) and image of actual assembled cell cap.
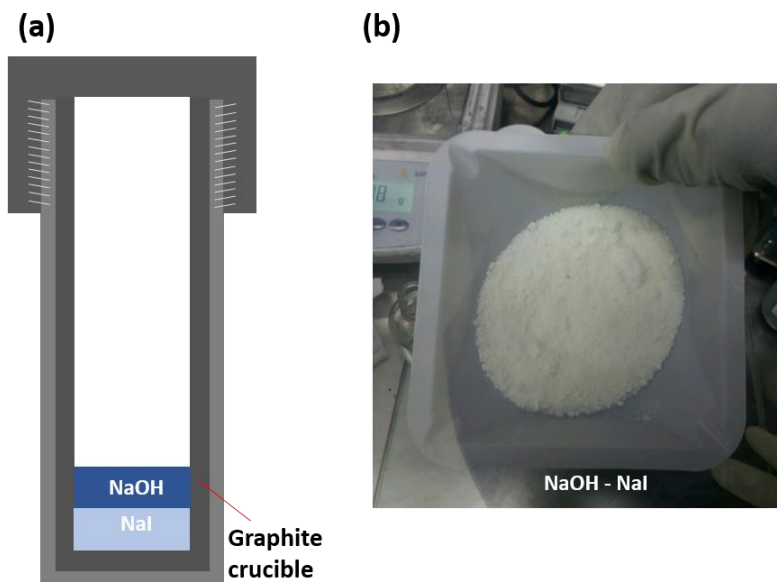
Figure 31. Part of manufacture process for NaOH-NaI salt. (a) is cross section after insertion of NaOH and NaI powder and (b) is manufactured NaOH-NaI salt.
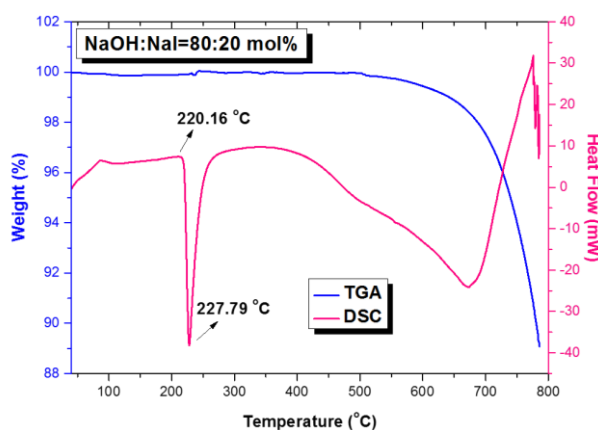
Figure 32. The results of thermogravimetric analysis and differential scanning calorimetry on manufactured NaOH-NaI salt. Endothermic reaction starts at 220.16 °C.

As shown in Figure 33(a), OCV change of Na‖Bi-Pb is described while heating up to 290 °C. OCV was saturated at 1.41 V, after that, the current of 1 mA was applied to the cell as shown in Figure 33(b). Possibility of charge and discharge were demonstrated, but voltage profiles were not stable. Especially, during charge, voltage profile was highly unstable because perhaps of unstable interface between each material. To stabilize the interface, operating temperature increased to 300 °C and then the current of 1 mA was applied. As shown in Figure 34(a), better stable voltage profiles were shown than before, discharge profile of 0.51 ~ 0.52 V, charge profile of 0.82~0.84 V.

It was speculated that Bi-Pb alloy using bulk Bi and Pb was probably not manufactured, consequently, it influences on unstable interface. Therefore, bulk Bi (T_m= 271 °C) was only used for cathode and then Na‖Bi cell was assembled. After that, the current of 3 mA was applied during charge and discharge at 280 °C as shown in Figure 34(b). Overpotential increased during cycling so it became impossible after the 8th cycle due to the overpotential.

51
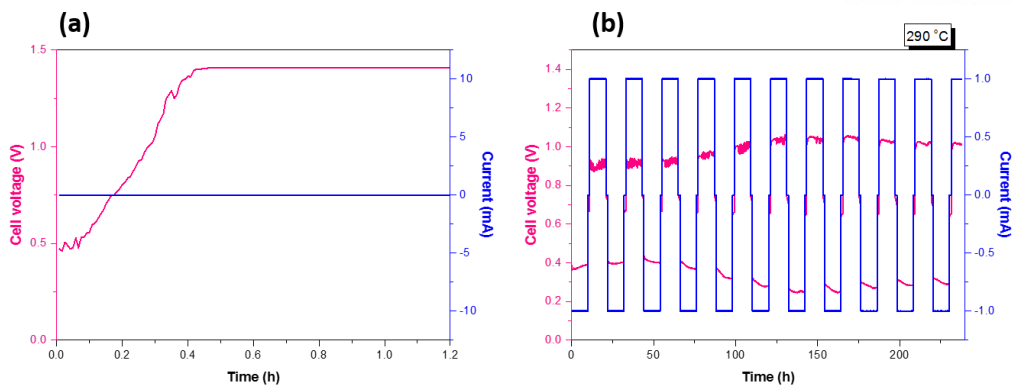
Figure 33. Electrochemical performance of Na|NaOH-NaI|Bi-Pb cell. The open circuit voltage change of Na|NaOH-NaI|Bi-Pb cell during heat up to 290 ºC in (a) and (b) is the result of galvanostatic cycling at 1 mA and 290 ºC.

Figure 34. Electrochemical performance of (a) Na|NaOH-NaI|Bi-Pb and (b) Na|NaOH-NaI|Bi cell. They were operated at 1 mA (300 ºC) and 3 mA (280 ºC), respectively.

High current was not applied to the Na||Bi-Pb and Na||Bi cell due to overpotential of them. The reason of increased overpotential is probably oxidation of liquid Na. As shown in Figure 35, (a) is before operation and (b) is after that. Difference of Na before and after is obvious. During the operation, oxidation of liquid Na occurred. Therefore, it is better to use Li as anode than to use Na in terms of reactivity although Li (T_m= 181 ℃) has higher melting point.

(a)

(b)
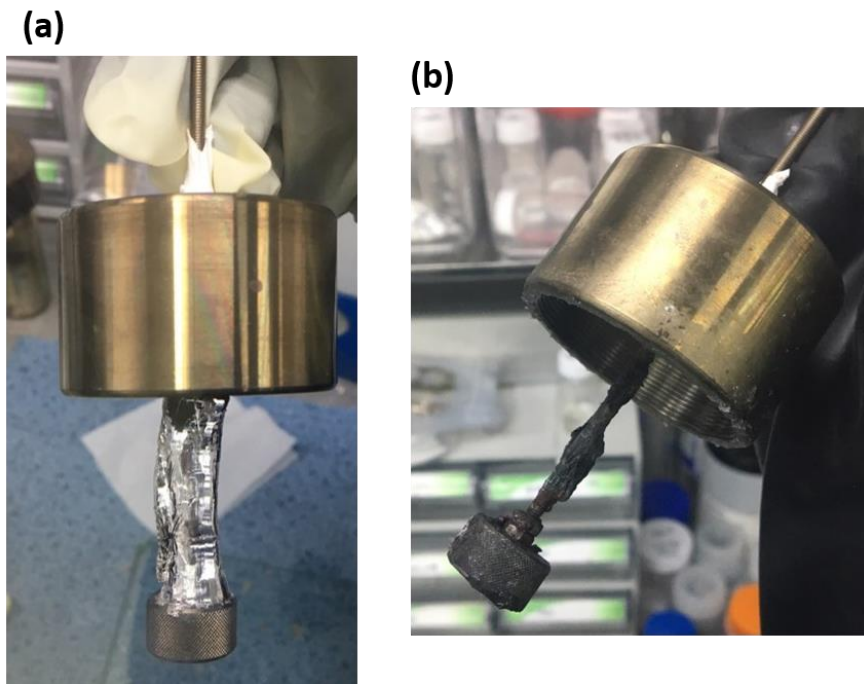
Figure 35. Image of combined cell cap and Na metal (a) before and (b) after operation. (a) showed clean surface of Na metal, but (b) has oxidized surface.

3.4. Fabrication and electrochemical performances of Li|LiCl-LiF|Bi cell

For high current rate of LMB cell, Li, Bi and LiCl-LiF of eutectic composition (70:30 mol%, T_m= 500 °C) were used as anode, cathode and electrolyte respectively. LiCl-LiF salt was prepared equal to manufacture process of $MgCl_2$-NaCl-KCl electrolyte. Powder LiCl (99 %, Alfa aesar) and LiF (98.5 %, Alfa aesar) salt were mixed and then those were inserted into crucible. Finally, it was heated at 600 °C for 20 hours. Manufactured salt was shown in Figure 36. Li (99.9 %, Alfa aesar) was used in the form of foil and assembly process is equal to Mg||Sb cell.

In Figure 37(a), OCV change of Li||Bi cell was shown with the temperature and it was stabilized at 0.94 V, 540 °C. When applying the current of 100 mA, results of charge and discharge profile are shown in Figure 37(b). Overpotential of first discharge was about 0.27 V and that of first charge was about 0.25 V. The shape of the first charge voltage was unstable probably because of the self-discharge and side reaction which are disturbing charge reaction. From 6th cycle, the voltage of charge and discharge gradually decreased and finally, in the 10th cycle, cell short occurred during discharge reaction. However, after the 10th cycle, the discharge was relatively constant than before the 10th cycle and the charge was still unstable. When 50 mA was applied to this cell, relatively stable shape of initial charge and discharge voltage is shown in Figure 38(a). In the 5th cycle, the overpotential of charge voltage increased and the discharge capacity decreased from the 18th cycle. This resulted in a galvanostatic charge and discharge which was the first long-term cycling performance that operated about 1600 h. In Figure 38(b), uneven capacity of charge and discharge led to irregular coulombic efficiency.
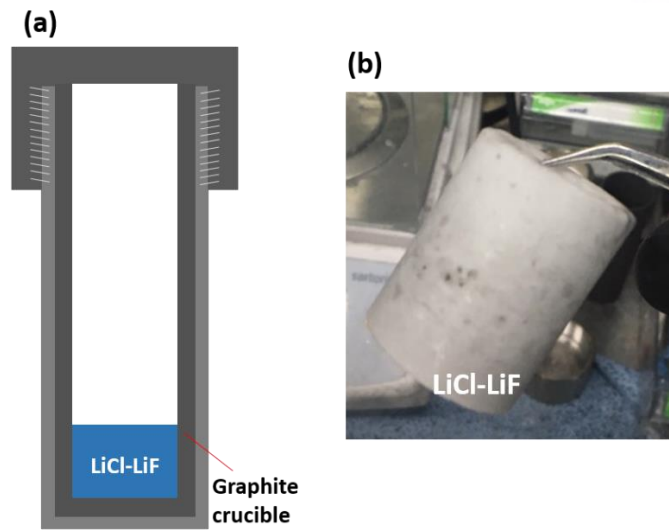
Figure 36. Part of manufacture process for LiCl-LiF salt. (a) is cross section after insertion of LiCl and LiF powder and (b) is manufactured LiCl-LiF salt.
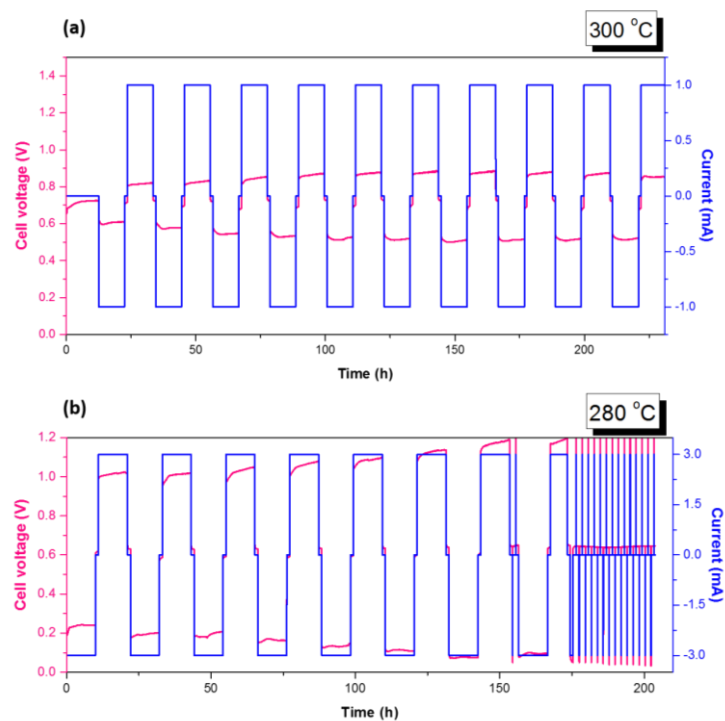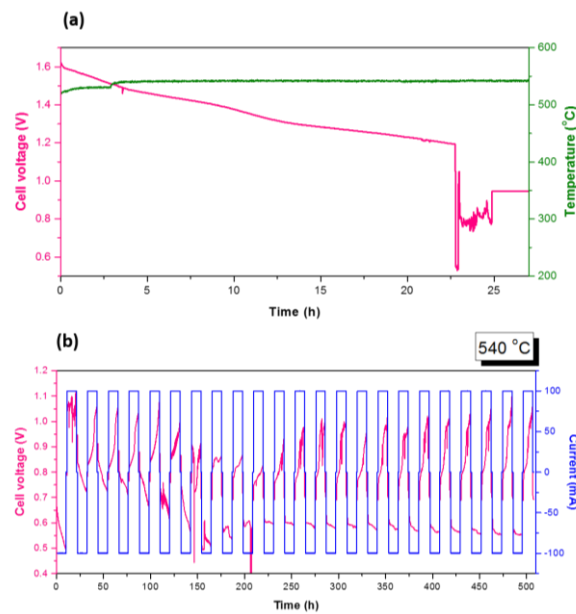

Figure 37. Electrochemical performance of Li|LiCl-LiF|Bi LMB cell. The open circuit voltage change of Li|LiCl-LiF|Bi LMB cell during heat up to 540 ºC in (a) and (b) is the result of galvanostatic cycling at 100 mA (540 ºC).
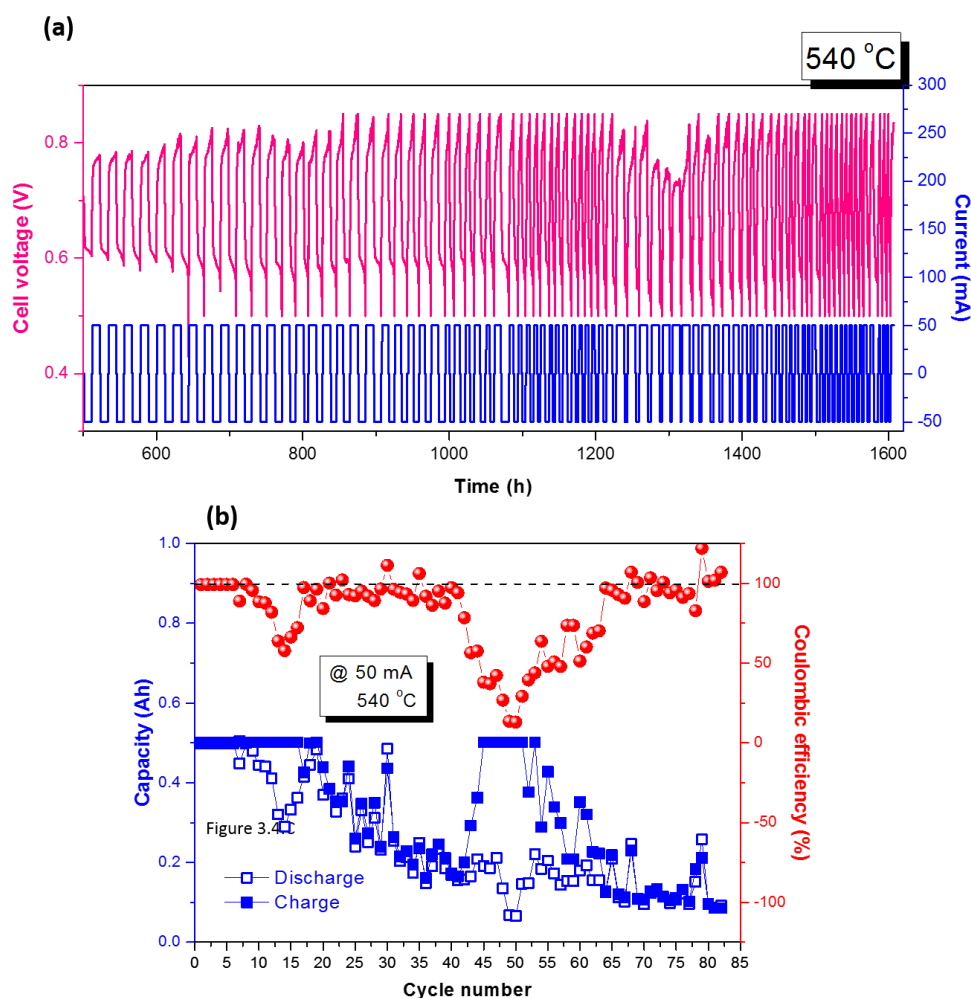
Figure 38. Electrochemical performance of Li|LiCl-LiF|Bi LMB cell. (b) is the result of galvanostatic cycling at 50 mA (540 °C) and (c) shows change of charge and discharge capacity and coulombic efficiency during cycling.

Although these were encouraging results, there were experimental problems on the Li||Bi cell. Most of all, the side reaction had a bad influence on electrochemical performance of the cell. Liquid Li spontaneously reacted with Al_2O_3 tube while making $LiAlO_2$, Li_4AlO_4 or Li_9Al_4.[50] When 100 mA was applied, OCV after charge and discharge was almost same as 0.69

V. It means the difference of chemical potential caused by Li concentration between anode and cathode was equal after charge and discharge, therefore Li was used for unwished reaction such as making $LiAlO_2$, etc. Thus, to avoid these reactions, using MgO or BN tube for insulator is encouraged. Carbon contamination on electrolyte induces cell short through self-discharge and increased electrical conductivity. Generally, electrical conductivity of graphite, which is based on carbon, is $7.837 \ 10^{-6} \ \Omega \cdot m$ and that means electrical conductor. Carbon deposition on electrolyte maybe makes path ways for electrons and consequentially, cell short occurs. Therefore, a newly modified LMB cell is required through removing harmful things.

3.5. Summary

Second LMB cell, without get rid of Na, β''-Al_2O_3, was designed as modifying first cell. While using it, electrochemical performance of Mg||Sb, Na||Bi-Pb, Na||Bi, and Li||Bi cell was measured. Operability was confirmed through each result of galvanostatic test, but there are several problems such as side reaction between liquid Mg and Al_2O_3, Na oxidation, side reaction of liquid Li, etc. Therefore, a new type of cell was needed to obtain more stabilized cycle performance. In the next section, the third designed LMB cell will be explained and then electrochemical performance and analysis will be elucidated.

4. Chapter 3. Third design of LMBs cell

4.1. Design and choice of cell components

SUS304 for cell cap, cell cup, negative current collector, and positive current collector was still used. However, graphite crucible and Al_2O_3 tube, which made side reaction, were removed from the cell. As removing Al_2O_3 tube, other materials or methods must come up for insulator to prevent cell short due to directly contact between anode and positive current collector. In addition, other materials or methods should not react with other components. MgO or BN tube is suitable for these requirements. However, if anode material dose not directly contact with positive current collector, the cell short will not come and there is no need to use an insulator. As shown in Figure 39, molten salt electrolyte can be used for electrical insulator by spacing out between anode and positive current collector. Liquid Li is confined in the Ni or Ni-Fe foam due to Ni reacted with Li. These new designed LMB cell simplifies assembly process, moreover, decreases the total cost of cell components through removing insulator and graphite crucible.

Cell cap and cup were prepared as a before design and, also, negative current collector was attached with cell cap using ceramic paste bond. Ni foam was fixed in negative current collector as shown in Figure 40(a) and then that was placed into full of liquid Li, which was melted in SUS304 crucible at 480 ºC, as shown in Figure 40(b). After about 15 hours, Li soaked Ni foam was completed as show in Figure 40(c). Cathode material and electrolyte powder (LiCl and LiF) were just inserted into cell cup. Finally, cell cap with negative current collector is combined with cell cup and then LMB cell is placed into measuring system.
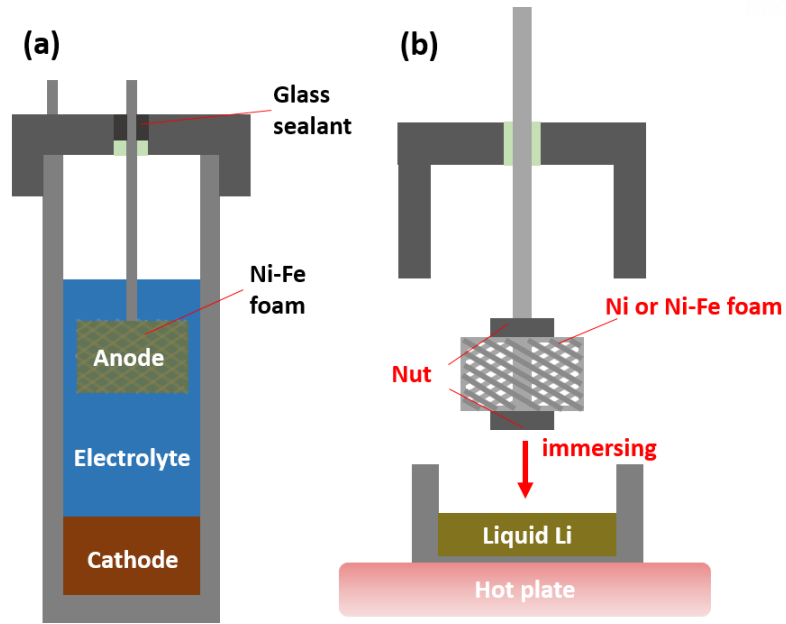
Figure 39. Schematic diagram of third desinged cell. (a) is expected cross section of third designed LMB cell after assembly and (b) is process of Li soaking in Ni foam.
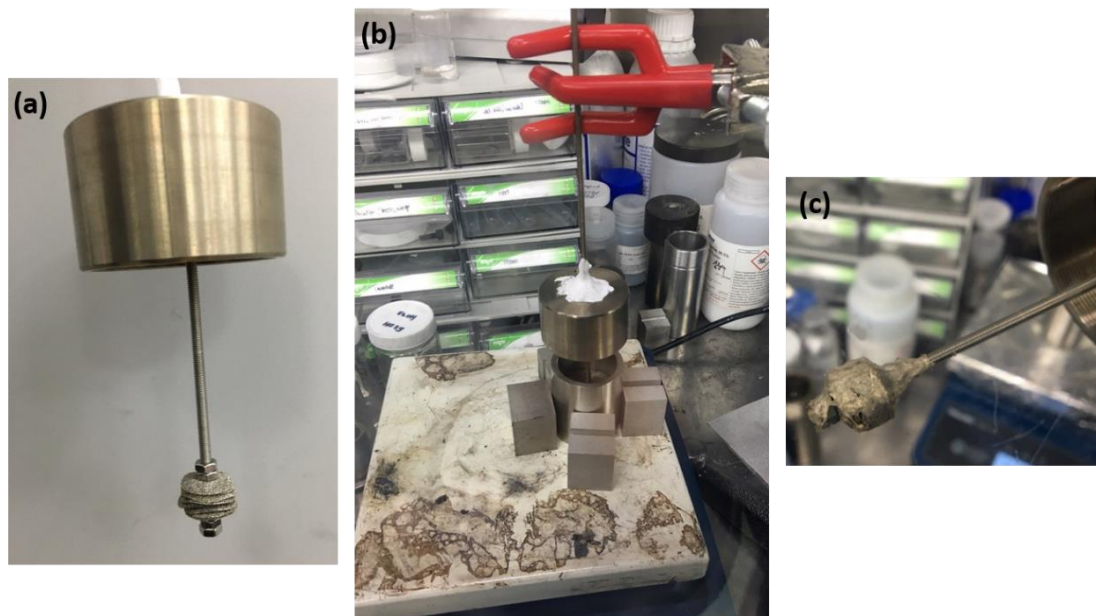
Figure 40. Image of actual process of Li soaking in Ni foam. (a) is prepared Ni-Fe foam combined with cell cap, (b) is image during soking, and (c) is after soaking.

4.2. Fabrication and electrochemical performances of Li|LiCl-LiF|Bi cell

Negative current collector with Li soaked Ni foam and cell cap were assembled with cell cup which included bismuth as cathode and LiCl-LiF as electrolyte. After raising the temperature, as shown in Figure 41(a), the OCV of a Li|LiCl-LiF|Bi cell was almost stabilized at about 1.03 V although it gradually decreased. When 100 mA was applied to a cell, Figure 41(b) shows galvanostatic charge and discharge at 360 ℃. Cut-off condition is 1h or 0.8 V during discharge and 1.1 V during charge. The result proved relatively stable charge and discharge voltage profiles than using a second cell. In Figure 42(a), change of capacity and coulombic efficiency in accordance with cycle is monotonous. In comparison with previous coulombic efficiency of a Li||Bi cell using second cell, that of a Li||Bi cell shows more efficient and more stable. Additionally, in Figure 42(b), change of OCV, after the charge and discharge talks, that very reversible reaction occurred during charge and discharge.
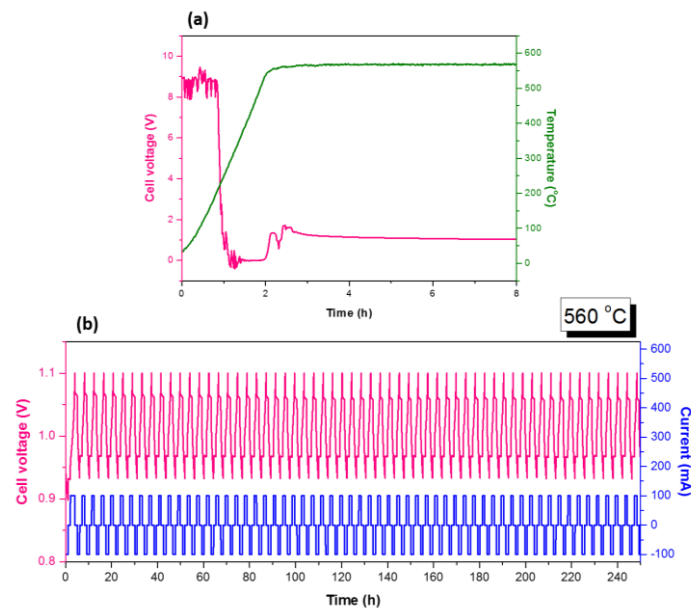
Figure 41. Electrochemical performance of Li|LiCl-LiF|Bi LMB cell. The open circuit voltage change of Li|LiCl-LiF|Bi LMB cell during heat up to 560 ºC in (a) and (b) is the result of galvanostatic cycling at 100 mA (560 ºC).

Figure 42. Electrochemical performance of Li|LiCl-LiF|Bi LMB cell. (a) shows change of charge and discharge capacity and coulombic efficiency during cycling and (b) is the OCV after 30 minutes after charge and discharge.

61
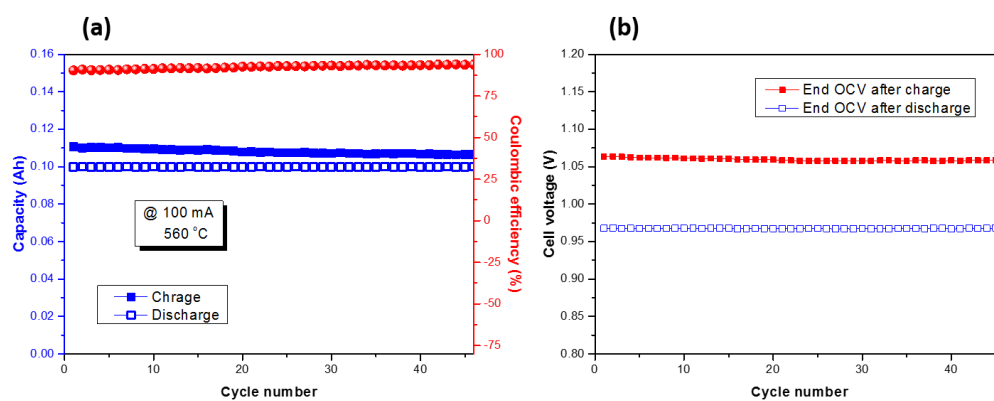
In order to confirm repeatability, galvanostatic charge and discharge test of second Li∥Bi cell was translated into action. Cell assembly process and preparation of material remain unchanged. In Figure 43(a), OCV of second Li∥Bi cell was measured in accordance with raised temperature. Unlike previous measurement of OCV, it gradually decreased was observed for a during relatively long time. After 8 hours, the OCV was about 1.01 V, however, a sharp decrease occurs from 13 hours to 15 hours than the previous decrement. Decrease of the OCV was steadily continued until applying the current. The Li∥Bi cell suffered from self-discharge which is harmful to storage efficiency such as capacity and energy. The current of 200 mA, which is 2 times higher than previous galvanostatic test, was applied to a cell. Cut-off condition is 0.85 V during discharge differed from previous cell and 1.1 V during charge. Figure 43(b) shows the result of galvanostatic cycle performance. Considering result, repeatability was corroborated through smooth charge and discharge voltage profile. However, change of capacity increased according to cycle as shown in Figure 44(a). On the contrary, coulombic efficiency was almost steady according to cycle pointing to 95~96 %. In Figure 44(b), which shows OCV after charge and discharge, OCV after discharge slightly decreased in accordance with cycle compared with OCV after charge. Associating it with capacity and coulombic efficiency results, more Li enters cathode on discharge according to cycle because overpotential of discharge voltage decreased. Therefore, discharge capacity continuously increased and charge capacity also increased in accordance to increased discharge capacity. The OCV means difference of chemical potential between anode and cathode, therefore, more inserted Li into cathode would be the reason of decreased OCV after discharge. The decreased overpotential could be originated from change of distance between anode and cathode. In Figure 45(a), the schematic diagrams express expected cross section image of the first state and after several cycles of Li∥Bi cell. Li entered in the place that is close to negative current collector during charge. After several cycles, the

distance between anode and cathode will be much closer. It means overpotential decreased after several cycles. If Li continues accumulating at tip of negative current collector, it causes cell short as directly connecting anode with cathode. It maybe comes from inappropriate Li soaked in Ni foam as shown in Figure 45(b).
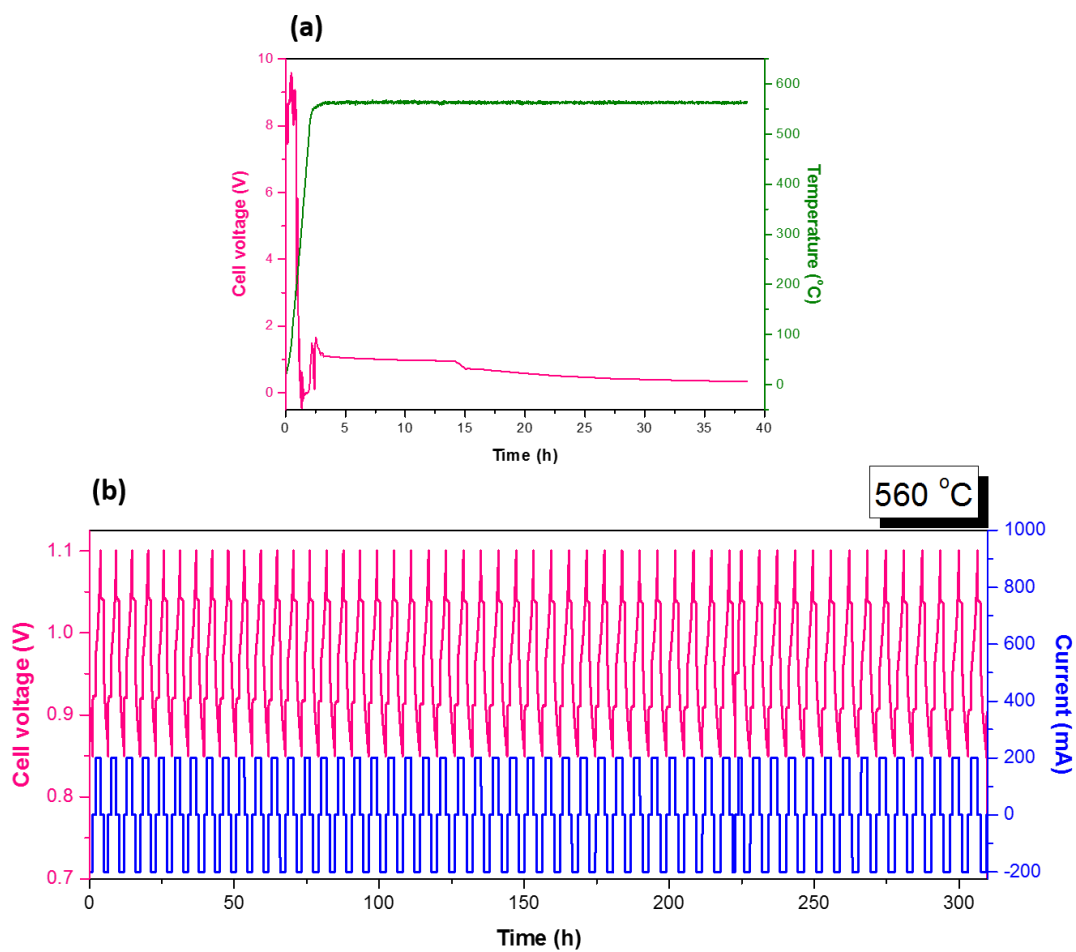
Figure 43. Electrochemical performance of Li|LiCl-LiF|Bi LMB cell. The open circuit voltage change of Li|LiCl-LiF|Bi LMB cell during heat up to 560 ℃ in (a) and (b) is the result of galvanostatic cycling at 200 mA (560 ℃).

Figure 44. Electrochemical performance of Li|LiCl-LiF|Bi LMB cell. (a) shows change of charge and discharge capacity and coulombic efficiency during cycling and (b) is the OCV after 30 minutes after charge and discharge.

Figure 45. Expected problems of Li|LiCl-LiF|Bi LMB cell. (a) Cross section of Li|LiCl-LiF|Bi LMB cell and (b) actual image after Li soaking.

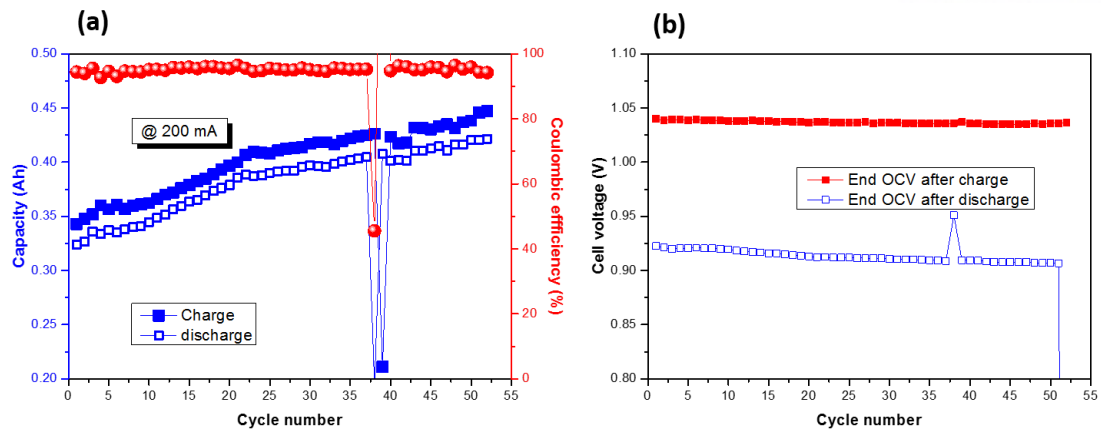## 4.3. Fabrication and electrochemical performances of Li|LiCl-LiI|Bi-Pb cell

As shown in Figure 46(a), Ni-Fe foam, which has thick thickness and bulky pores, was used as negative current collector to smoothly absorb liquid Li than Ni foam. As shown in Figure 46(b), it was appropriately cut and then combined with negative current collector bar using a nut. Finally, the space between the nut and negative current collector bar was welded to fix them. Liquid Li was soaked in Ni-Fe foam at 480 ℃ and the real shape of that shown in Figure 46(c). Liquid Li was totally soaked in Ni-Fe foam through the shape of surface and cross section image. Bi-Pb of eutectic composition alloy was used as cathode. In the case of using Pb as alloy element, it doesn't participate in reaction with Li and it decreases the melting temperature of cathode. In addition, it doesn't disturb the cell voltage during charge and discharge.[51,52] LiCl-LiI (36:64 mol%, T_m= 371 ℃) of eutectic composition, which was selected as electrolyte, has not been reported as electrolyte of LMB. DSC and TGA measurements of LiCl and LiI are shown in Figure 47. Through these results, melting point of LiCl (99.995 %, T_m= 605 ℃, Alfa aesar) and LiI (99.95 %, T_m= 469 ℃, Alfa aear) were confirmed. Before endothermic reaction regarded as melting point, they have another endothermic reaction. Those are probably caused by moisture and residue organic materials. LiCl-LiI were manufactured using quartz crucible in furnace. Heating process is as follows.

Heating process: 80 ℃, 10 h → 260 ℃, 10h → 450 ℃, 3h → room temperature

First and second step mean removing residue moisture and organic materials. LiCl and LiI were homogeneously mixed at 450 ℃. Through DSC and TGA measurement as shown in Figure 48, melting point of LiCl-LiI was confirmed. Before endothermic reaction at 368.63 ℃, three peaks mean moisture and organic residues. Assembly process was equal to Li||Bi cell.

Figure 46. Images of (a) comercialized Ni-Fe foam, (b) Ni-fe foam combined with negative current collector using thread and nut, and (c) surface and cross section after Li soaking.

Figure 47. The results of TGA and DSC on (a) LiI and (b) LiCl salt. In result of (a), 80.32 °C, 132.21 °C, and 320.07 °C as endothermic reaction mean removing of moisture and residue organic waste. In result of (b), 79.73 °C, also, means removing of moisture.

Figure 48. The results of TGA and DSC on manufactured LiCl-LiI salt. 66.23 ℃, 77.60 ℃, and 127.75 ℃ as endothermic reaction mean removing moisture and residue organic waste. Endothermic reaction at 368.63 ℃ means melting point of LiCl-LiI.

While heating the cell up to 410 ℃, the OCV of a Li‖Bi-Pb cell was measured as shown in Figure 49(a) and it continuously decreased, but it was nearly saturated at 0.72 V. The current of 500 mA (~52 mA cm⁻¹) was applied to cell during galvanostatic charge and discharge test and the cut-off condition was 0.4~1.1 V. charge. The discharge profile of 1st, 20th, 30th, 40th, and 86th are shown in Figure 49(b). In the first cycle, capacity was about 1 Ah. If Li reacted only with Bi of Bi-Pb alloy, Li was inserted about 48 mol% in comparison with Bi mole fraction. According to the previous research paper, at 550 ℃, in Li|LiCl-LiF|Bi LMB cell, Li was inserted about 70 mol% in comparison with Bi. Consequently, quantity of inserted Li is lower in case of Li‖Bi-Pb than Li|LiCl-LiF|Bi maybe because of the operating temperature. However,

lower operating temperature is benefit for thermal management. As shown in Figure 50, from 1st cycle to about the 40th cycle, capacity of charge and discharge decreased to about 0.8 Ah, but coulombic efficiency was nearly 99 %. In comparison with voltage profile of 1st cycle and 40th cycle as shown in Figure 49(b), capacity of slope area where the one phase has a reaction, in which liquid phase was made by the insertion of Li into Bi, take places was nearly not changed. However, that of plateau where the two phases have a reaction, in which solid phase is produced from liquid phase, take place decreased. After the 40th cycle, the capacity of that gradually increased and then the capacity decreased and the healing was repeated. Overall, coulombic efficiency showed about 99.3 % which means the discharge and charge capacity have high rate of concordance.
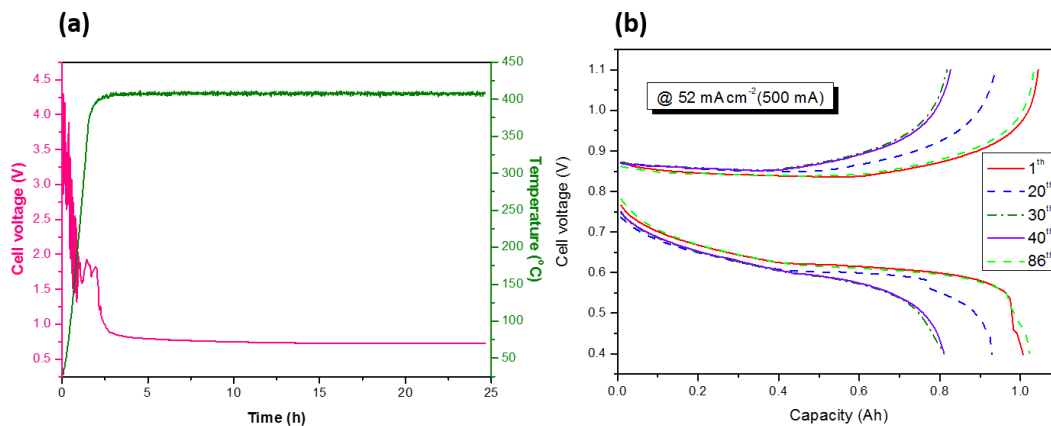
Figure 49. Electrochemical performance of Li|LiCl-LiI|Bi-Pb LMB cell. The open circuit voltage change of Li|LiCl-LiI|Bi-Pb LMB cell during heat up to 410 ℃ in (a) and (b) shows voltage profiles, which is 1st, 20th, 30th, 40th, and 86th, of discharge and charge at 500 mA (410 ℃).
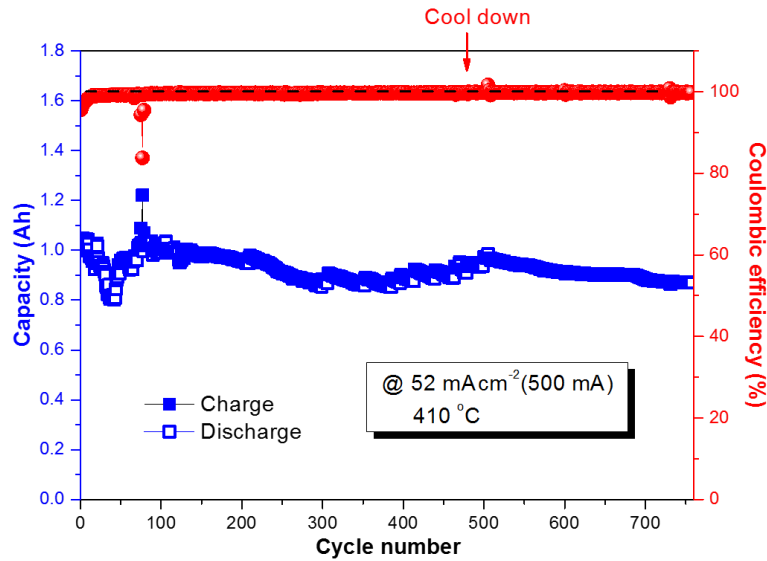
Figure 50. Change of charge and discharge capacity and coulombic efficiency of Li|LiCl-LiI|Bi-Pb LMB cell during cycling.

Additionally, among several LMB cell tests up to now, Li||Bi-Pb cell has been operated above four months. Therefore, the cool down test, which is a test for practical application, proceeded as follows.

    (1) Cut off the power of furnace, but Ar gas flowing is maintained

    (2) Check temperature down to room temperature, again heating the cell up to operating

        temperature

    (3) Electrochemical performances such as galvanostatic result are compared to previous

        one.

The reason of investigating the cool down test of the cell is to that consider the real EESDs. If

the device for maintaining temperature breaks down, we have to examine whether the electrochemical properties of the cell will be largely changed or not. At about 479th cycle, above the mentioned process proceeded. As shown in Figure 51(b), change of OCV was measured during the process. At room temperature, OCV was about 0.87 V with little fluctuation, during increasing temperature, it was recovered as well as before cutting off the power. When operating the cell, capacity and coulombic efficiency had almost the same value as shown in Figure 51(a). Therefore, the electrochemical properties of Li‖Bi-Pb cell were not fallen although unexpected cool down does occurs.
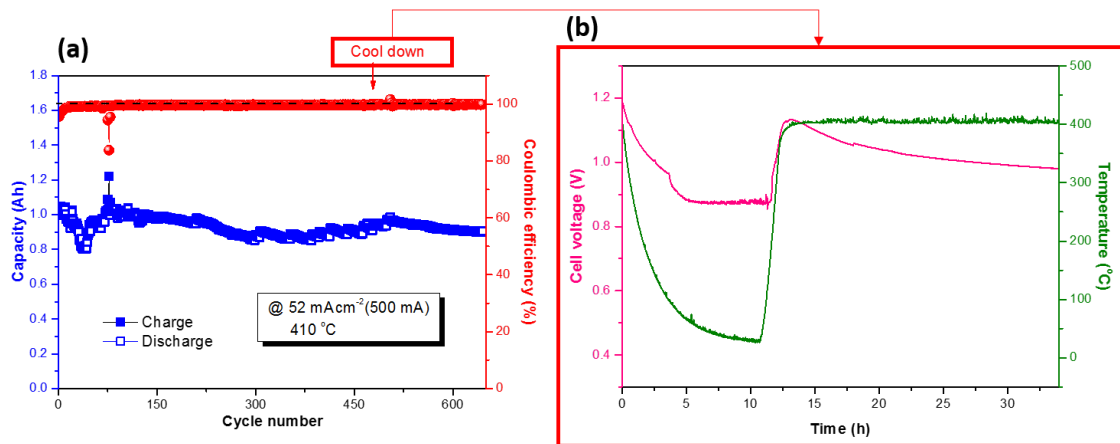
Figure 51. The result of cool down test of Li|LiCl-LiI|Bi-Pb. (a) shows coulobic efficiency and change of charge and discharge capacity before and after cool down test. (b) shows The OCV change after cool down to room temperature and before heat up to 410 °C (operating temperature).

Cyclic voltammetry (CV) was measured to examine indirect internal resistance and whether charge and mass transport is easy or not. On the contrary to Li ion half-cell test, as shown in Figure 52(a), linear profile of CV result means that internal resistance constantly increases.[53] As shown in Figure 52(b), Electrochemical impedance spectroscopy (EIS) indicates negligible charge transfer resistance because there is no clear semi-circle. In addition, Li|LiCl-LiI|Bi-Pb cell has relatively lower ohmic resistance of about 0.2 Ω. Through these results, charge and

mass transport were smoothly accomplished due to using all liquid materials as anode, cathode, and electrolyte. Therefore, in accordance with that result, high rate capability is a possibility.

Leakage current, which is an indicative of degree of self-discharge, were measured through stepped-potential method as shown in Figure 52(b). After charge, the OCV was saturated about 0.9 V and then 0.9 V was persisted until the current density is saturated at 0 mA cm^{-2} which means the charge and discharge were stopped. After that, 1.1 V was applied and then saturated current density was taken. It was about 0.05 mA cm^{-2} which is a very lower value than previous reported research on Mg|MgCl$_2$-NaCl-KCl|Sb (0.4 mA cm^{-2}). In addition, 1.2 V was applied and then saturated current density indicates about 0.4 mA cm^{-2}. It means the leakage current increase more than before because of the over-charge. Consequently, LiCl-LiI is suitable for electrolyte of LMB due to very low value of self-discharge.
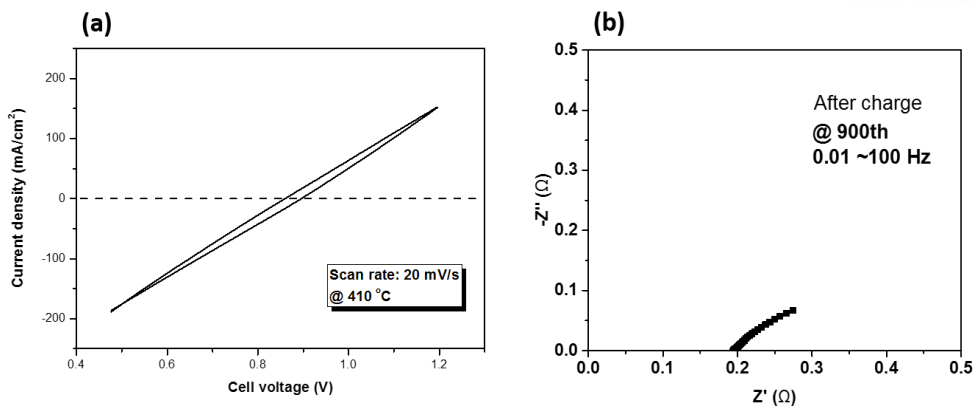
Figure 52. Electrochemical characterization of Li|LiCl-LiI|Bi-Pb LMB cell. Scan rate of cyclic voltammetry (CV) is 20 mV s^{-1} @ 410 °C and result of CV shown in (a). (b)Electrochemical impedance spectrascopy for measuring ohmic and charge transfer resistance @ 900th cycle. Voltage amplitude of 0.1 V rms and frequency range of 0.01 to 100 Hz.
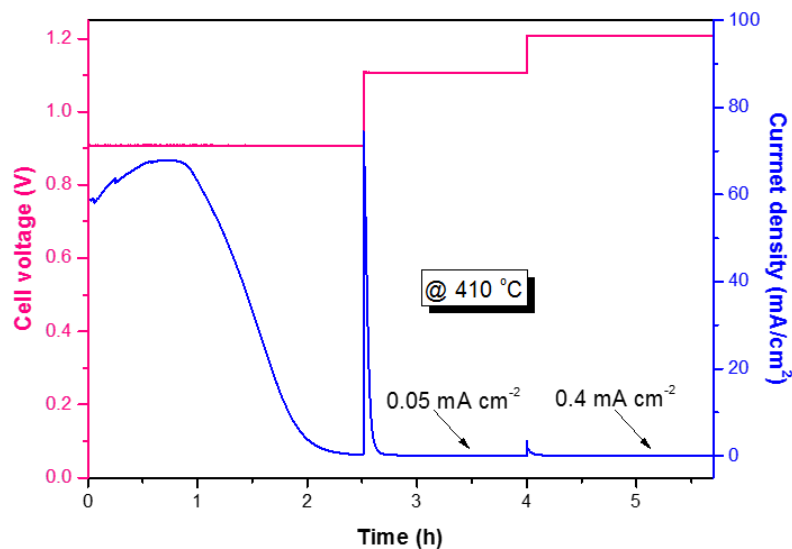
Figure 53. The leakage current was measured by stepped-potential method while applying constant potential, which were 1.1 V and 1.2 V, above OCV.

As shown in Figure 53(a), when stopping Ar gas flowing, capacity of Li‖Bi cell went down. When measuring of the OCV ended, there was also a decreased after several cycles as shown in Figure 53(b). Through these results, it was speculated that Ar gas did not stay in quartz tube. Therefore, capacity fading occurred due to possible reactions between air and inner materials. It means the cell structure was unstable in the air. In addition, more modifications are needed to be operated in air. In the future, to suppress degradation of electrochemical performance, closed system, which means no correspondence between inside of the cell and the outside air, must be fabricated. Therefore, as shown in Figure 54, welded LMB cell was designed. Each contact surface between cell cap and cup should be welded. Additionally, the space between negative current collector and Al_2O_3 tube should be filled by epoxy resin.[54] After assembly, inside gas of cell is pulled out through valve line using vacuum pump and then fresh Ar gas will be filled out. According to these processes, side reaction will probably not be a concerned.
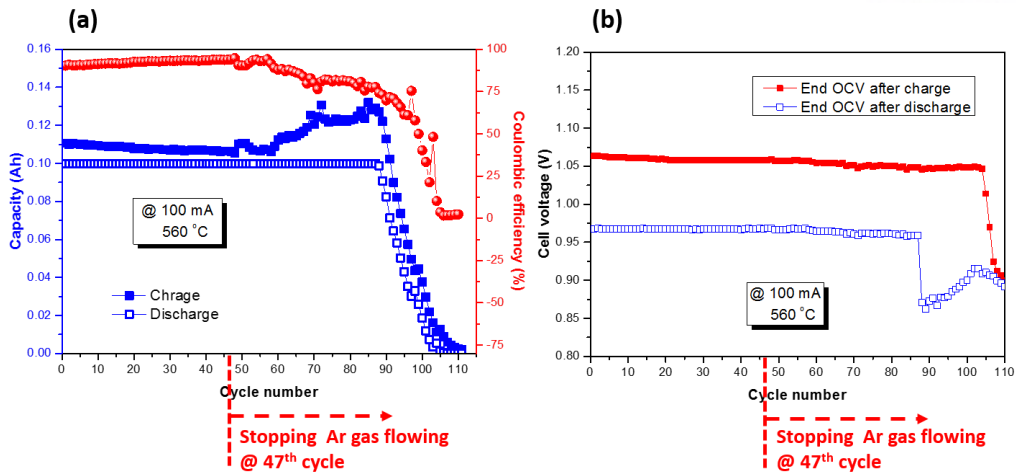
Figure 54. Change of electrochemical perfomance of Li|LiCl-LiF|Bi LMB cell before and after stopping Ar gas flowing at 47th cycle. (a) shows coulombic efficiency and charge and discharge capacity. (b) shows the OCV after 30 minutes after charge and discharge.
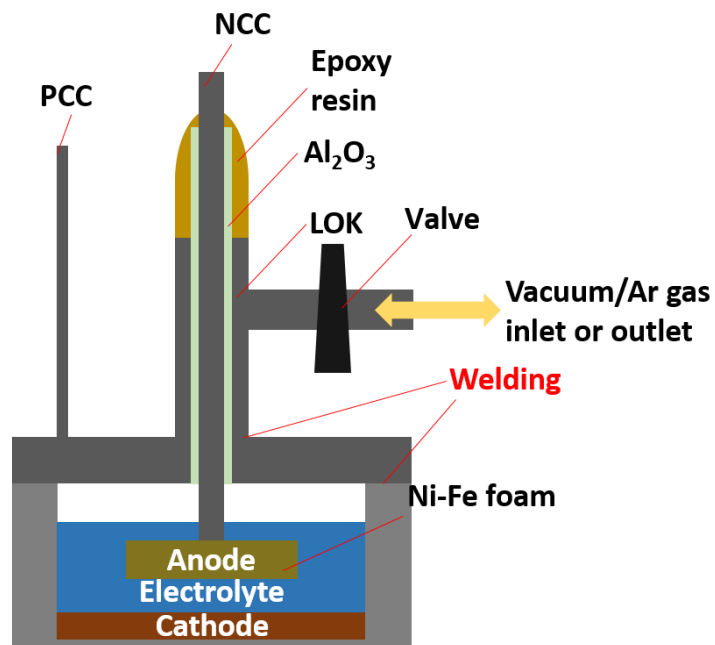
Figure 55. The components and cross section of further modified LMB cell (welded cell) in the furture work.

74

4.4. Summary

The third design of cell was completed as removing several components such as inner insulator and graphite crucible. Ni and Ni-Fe foam were used for making Li soak a negative current collector tip. Cycle ability of the Li|LiCl-LiF|Bi cell had better improvement than using a second designed cell because the contamination of electrolyte and side reaction was removed. In this section, LiCl-LiI salt was firstly used as electrolyte for the Li||Bi-Pb cell. It showed outstanding long-cycle ability, high coulombic efficiency, and low leakage current. The third designed cell is optimized under Ar gas flowing. Therefore, more improved cell design such as introduced welded cell will be required to test in the air.

5. Conclusions

EES system and devices have been received attention. Among various devices, EEDSs, such as LIBs, RFBs, Na-S batteries, etc, have been widely developed and researched. Liquid metal batteries have been examined as target for EESDs because of their benefits. However basic cell structure and measurement system were not totally released, therefore, measuring electrochemical performance of materials was not easy. In accordance with these requirements, design and fabrication of standard LMB cell components were studied in this thesis.

To set up standard cell components of LMBs, cell design, assembly, and electrochemical testing were repeated. Basic cell (first designed cell) of LMBs was designed based on hydrothermal autoclave which has been widely used for materials synthesis. Customized furnace for heating assembled cell was designed and fabricated. In addition, Ar gas flow system was equipped on furnace to make an inert atmosphere around a cell. Assembly process was appropriately devised once a new cell was designed. Basically, the galvanostatic cycle test took place in an assembled cell to analyze operability and electrochemical performance.

Through galvanostatic test of the Na|Na, β"-Al$_2$O$_3$|Sn cell using first designed cell, applying current of 1 mA to the Na||Sn cell at 300 $^\circ$C, Operability was assured. However, when applying current of 20 mA, the fracture of Na, β"-Al$_2$O$_3$ occurred owing to low wettability between liquid Na and Na, β"-Al$_2$O$_3$. In addition, high vaporization of liquid Na has bad influences on the cycle performance. Therefore, the second cell was designed as removing Na, β"-Al$_2$O$_3$ and adding graphite crucible and ceramic insulator such as Al$_2$O$_3$, BN, and MgO tube.

The Mg|MgCl$_2$-NaCl-KCl|Sb, Na|NaOH-NaI|Bi-Pb, and Li|LiCl-LiF|Bi cells were tested using second designed cell. Galvanostatic cycle test of the Mg||Sb cell was operated at 680 $^\circ$C while the current of 20 mA and 50 mA were applied during charge and discharge for 10 hours, respectively. Five cycles were accomplished at 50 mA, but gradually the voltage profile

decreased and, eventually, the cell short in the 6th cycle occurred probably because of a similar or higher density of anode and electrolyte. It comes from the side reaction between Mg and Al_2O_3 insulator. To solve these problem, the Na||Bi-Pb cell was introduced because of certain difference of density and no reaction between Na and electrolyte. Galvanostatic cycle test of this was operated at 300 °C while the current of 1 mA was applied to it during charge and discharge for 10 hours, respectively. The result showed relatively stable voltage profile but, when applying current of 3 mA, overpotential continuously increased because liquid Na was easily oxidized. Liquid Li, which has lower degree of oxidation than liquid Na, was used as anode material for the Li||Bi cell. Applying the current of 50 mA and 100 mA to it at 540 °C under cut-off condition of 10 hours, the galvanostatic cycle test of this was measured. Long-term cycling performance (>65 cycles) was achieved at 100 mA, however, capacity fading occurred probably because of contamination of electrolyte which increases value of solubility. Through the second designed cell, relatively higher rate capability and long-term cycling performance were achieved. On the other hand, problems still harass electrochemical performance of the cell. Graphite crucible and insulator were tossed out to avoid the contamination and the side reaction. Plus, Ni or Ni-Fe foam, in which liquid Li was soaked, was used for negative current collector tip.

Using a third designed cell, Galvanostatic cycle tests of the Li|LiCl-LiF|Bi and Li|LiCl-LiI|Bi-Pb were conducted at 560 °C and 410 °C respectively while the current of 100 mA, 200 mA were applied to the Li||Bi cell. In the case of Li||Bi-Pb, 500 mA was applied. Both cells were showed relatively stable cycling performance than previous cells which used second designed cell. Especially, the Li||Bi-Pb cell was being operated with a lower temperature than others which used liquid Li anode. Additionally, it has high rate capability (500 mA), long lifespan (>750 cycles, still operating) and high coulombic efficiency (>99.3%). Plus, CV, EIS,

stepped-potential measurement, and the cool down test were measured to analyze charge and mass transport of inner materials, value of self-discharge, and preservation of properties, respectively. It showed qualitatively fast charge and mass transport, low value of self-discharge (0.05 mA cm^{-2}), and preserves properties such as capacity and coulombic efficiency.

Without Ar gas flowing during operation, the galvanostatic performance deteriorated during the cycling. This could be perhaps because of reaction between inner materials and the air. Therefore, in future, the introduced closed system of LMB cell will be examined.

6. Appendix A

In this appendix, typical trial and error will be described about Na|Na, β"-Al$_2$O$_3$|Sn cell. As shown in Figure A-1, OCV was stabilized at about 1.38 V, however, sudden voltage drop occurred. It was probably caused by high polarization during discharge. When liquid Na was inserted into liquid Sn, mass of that decreased, therefore, reaction area will be reduced as shown in Figure A-2(a) and (b). It means current density gradually increased as shown in Figure A-2(c) and then finally, it induced higher resistance which means higher polarization. To improve these problems, mass of loading Na have to increase.
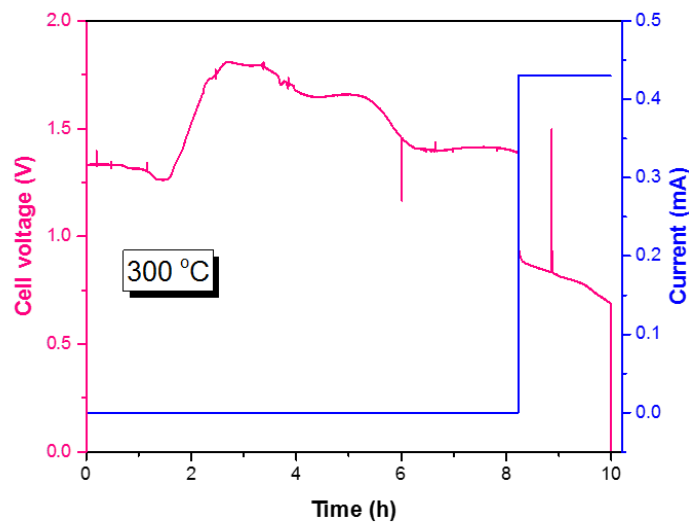
Figure A-1. Open circuit voltage and discharge profile of Na| Na, β"-Al$_2$O$_3$|Sn cell. Discharge at 0.43 mA and 300 ºC
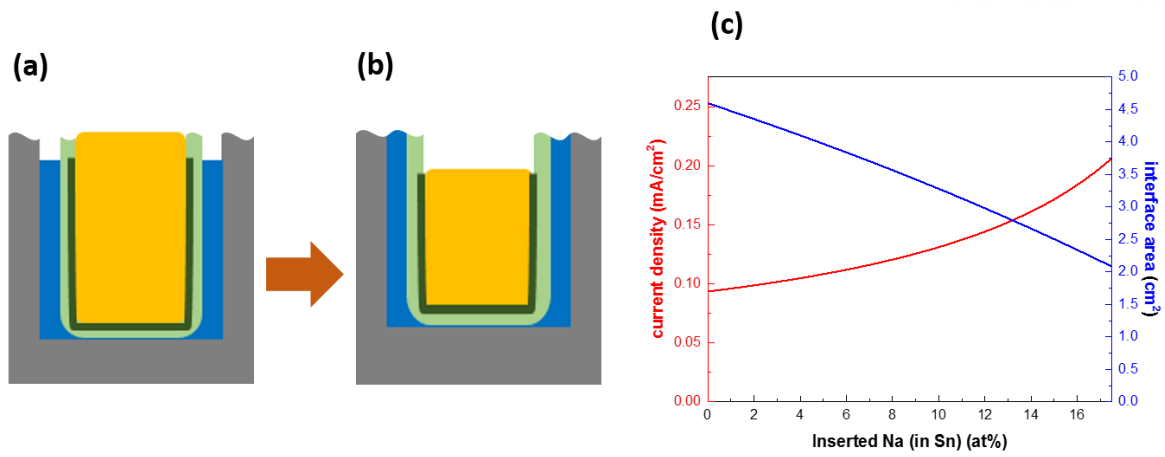
Figure A-2. Schematic diagram (a) and (b) show expected cross section of Na| Na, β"-Al$_2$O$_3$|Sn cell during discharge. (c) shows change of current density according to that of interface area (green line in (a) and (b)).

7. Appendix B

Typical trial and error will be described about Mg|MgCl$_2$-NaCl-KCl|Sb cell. When using mixed power of MgCl$_2$, NaCl, and KCl, instead of OCV stabilizing, short circuit occurred as shown in Figure B-1. On the contrary, as shown in Figure 25, OCV of the cell was stabilized as using manufactured MgCl$_2$-NaCl-KCl. As a result, it was experimentally confirmed that the self-discharge was little when the electrolyte was manufactured in advance.
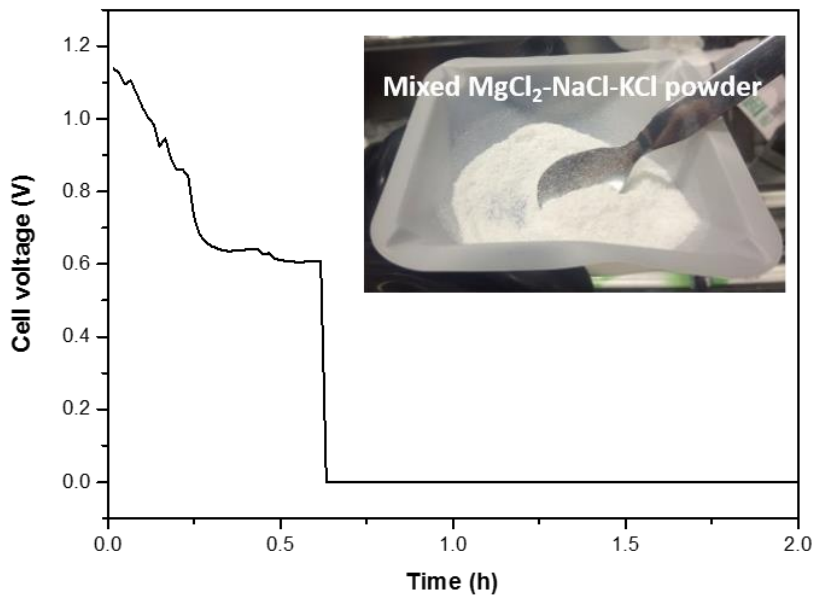
Figure B-1. OCV of Mg|MgCl$_2$-NaCl-KCl|Sb cell while raising temperature up to 680 ℃.

In order to obtain the results as shown in Figure 34, gavanostatic charge and discharge tests were experimented using Na as anode and NaOH-NaI as electrolyte. Judging from the fact that the bulk Bi and Pb were not mixed, powder Bi and Pb were used for making alloy. However, as shown in Figure B-2(a), alloy was not manufactured. The result, which is galvanostatic charge and discharge as shown in Figure B-2(b), was also difficult to interpret.

In response to these results, tin (Sn) was used for cathode to make stable liquid-liquid interface between electrolyte and cathode. Powder Sn was melted after it was placed into cell cup as shown in Figure B-3(a). Problem arising from using bulk Bi and Pb was solved as using a single metal as shown in Figure B-3(b). However, as shown in Figure B-3(c), the result of galvanostatic charge and discharge test is difficult to interpret same as before.
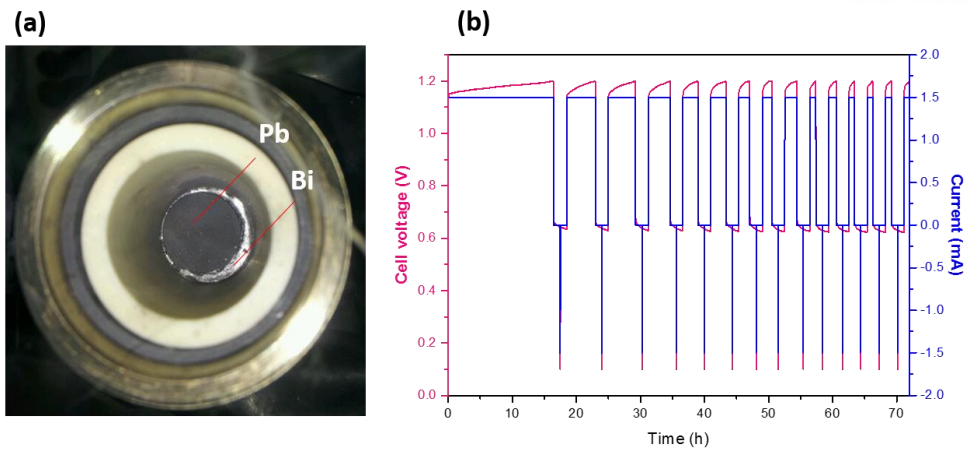
Figure B-2. (a)Bi and Pb in the cell cup after heat-treatment and (b)galvanostatic charge and discharge cycling of Na|NaOH-NaI|Bi-Pb cell at 390 ºC.
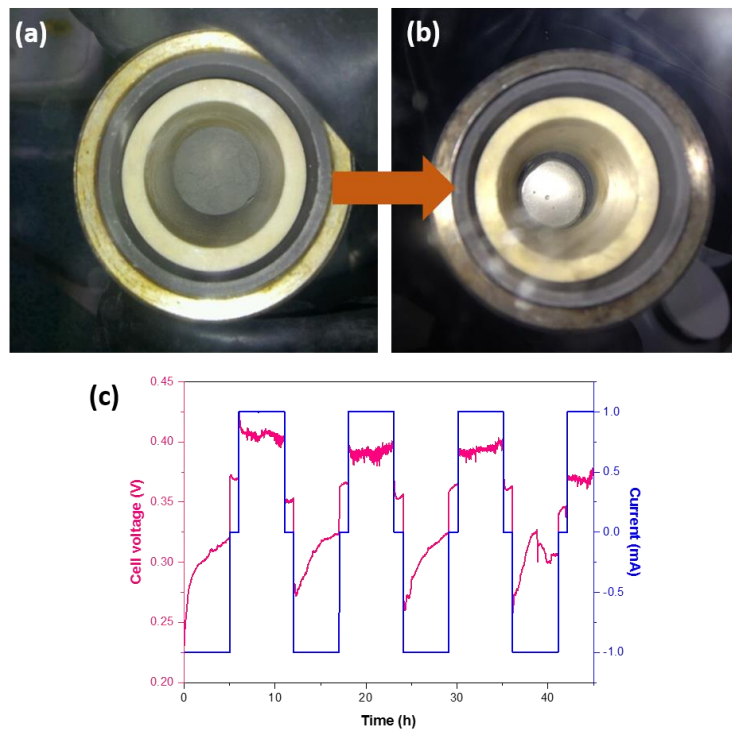
Figure B-3. (a) Sn powder in cell cup, (b) melted and cooled Sn, and (c) gavanostatic charge and discharge cycling of Na|NaOH-NaI|Sn cell at 320 ºC.

8. Appendix C

Ni-Fe foam was used for negative current collector tip in third designed cell. Condition of soaking liquid Li into the foam is important because it is directly associated with electrochemical performance. As shown in Figure C-1(a), in case of poor soaked Li, it gave a hard-to-interpret result. Therefore, to make a foam with Li well soaked, immersing process should conducted at above 150~200 °C higher than melting temperature of Li. As a result, well soaked foam was obtained as shown in Figure 46(c).

Process of manufacturing salt is important to electrochemical performance because it is related with self-discharge. For example, when LiCl-LiI salt was manufactured under unstable sealing, the appearance of salt looks dirty as shown in Figure C-2(a). As a result, using it as electrolyte for a Li|LiCl-LiI|Bi-Pb cell, sharp decrease of charge voltage occurred probably due to high degree of self-discharge of electrolyte. To avoid these problems, quartz tube was introduced. Sealing between salt and outside air was accomplished through quartz welding. Therefore, as shown in Figure C-3, relatively clear salt was manufacture.
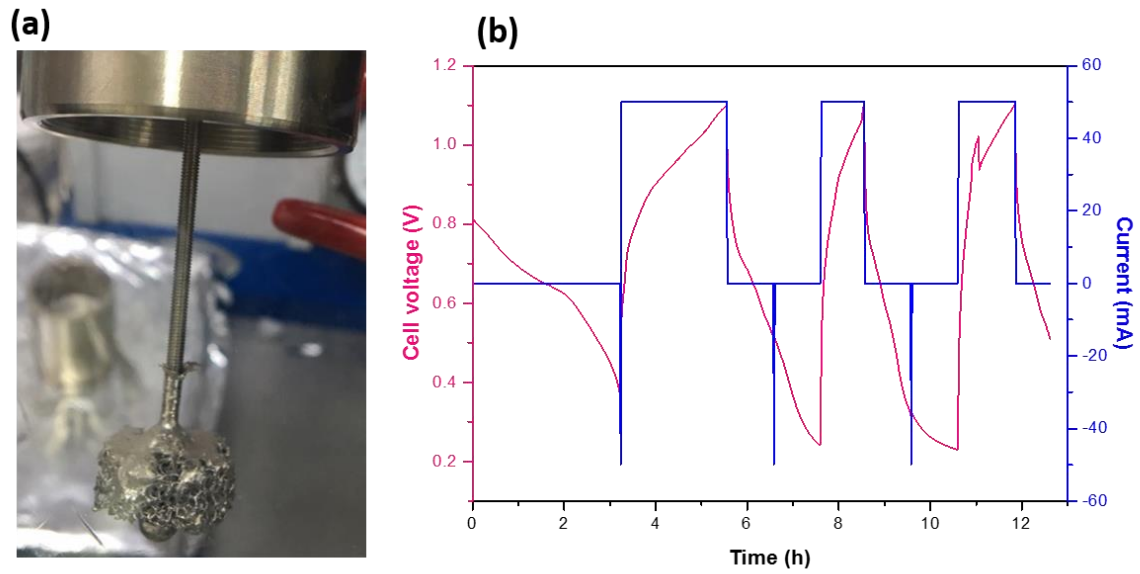
Figure C-1. (a)Li soaked Ni-Fe foam and (b)galvanostatic charge and discharge cycling of Li|LiCl-LiF|Bi at 560 ºC and current of 50 mA.
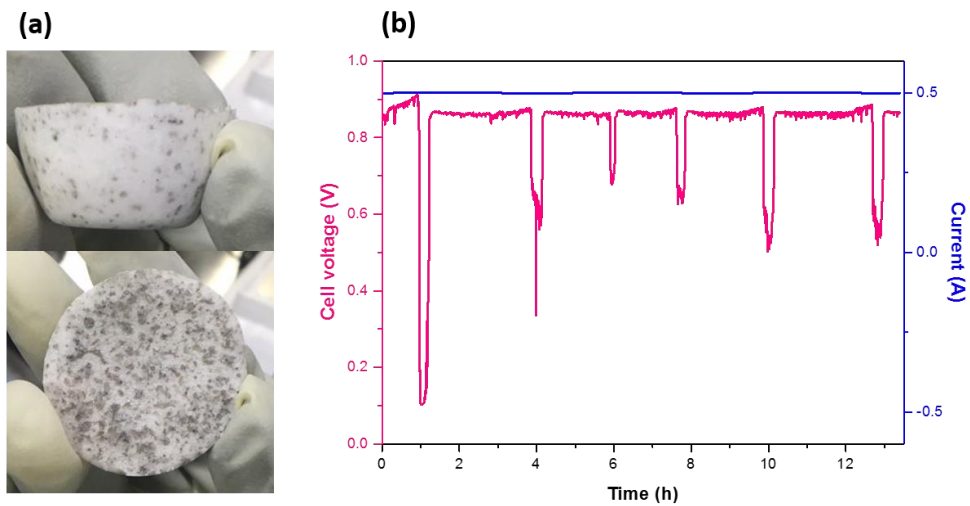
Figure C-2. (a)Manufactured LiCl-LiI salt and (b) galvanostatic charge test of Li|LiCl-LiI|Bi-Pb at 410 ºC and current of 0.5 A.
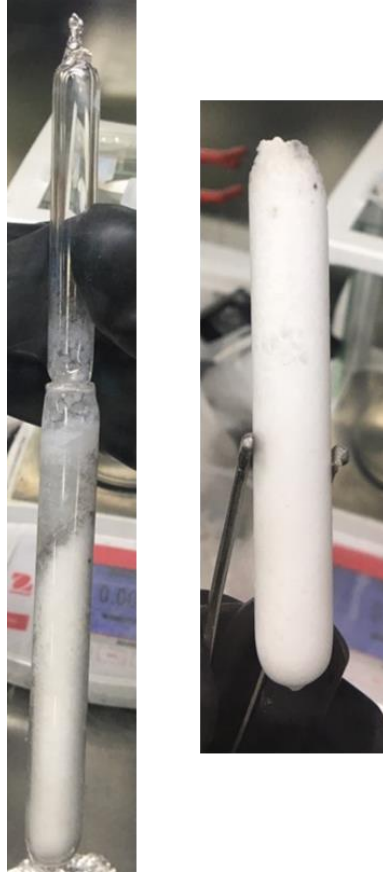
Figure C-3. Manufactured LiCl-LiI salt using quartz tube.

9. References

[1] Xian, L.; Jihong, W.; Mark, D.; Jonathan, C., Overview of current development in electrical energy storage technologies and the application potential in power system operation. *Applied Energy* **2015**, 137, 511-536.

[2] Dresselhaus, M.; Thomas, I., Alternative energy technologies. *Nature* **2001** 414, 332-337.

[3] Yang, Z.; Zhang, J.; Kintner-Meyer, M. C.; Lu, X.; Choi, D.; Lemmon, J. P.; and Liu, J., Electrochemical energy storage for green grid. *Chemical Reviews* **2011**, 111, 3577-3613.

[4] Cavallo, A., Controllable and affordable utility-scale electricity from intermittent wind resources and compressed air energy storage (CAES). *Energy* **2007**, 32, 120-127

[5] Bolund, B.; Bernhoff, B.; Leijon, M., Flywheel energy and power storage systems. *Renewable and Sustainable Energy Reviews*, **2007** 11, 235-258.

[6] Deane, J. P.; Gallachoir, B. P.; McKeogh, E. J., Techno-economic review of existing and new pumped hydro energy storage plant. *Renewable and Sustainable Energy Reviews* **2010**, 14, 1293–1302

[7] Dunn, B.; Kamath, H.; Tarascon, J.-M.; Electrical energy storage for the grid: a battery of choices. *Science* **2011**, 334, 928-935.

[8] Roberts, B.P.; Sandberg, C., The Role of Energy Storage in Development of Smart Grids. *Proceedings of the IEEE* **2011**, 99, 1139-1144

[9] Alotto, P.; Guarnieri, M.; Moro, F., Redox flow batteries for the storage of renewable energy: a review. *Renewable and Sustainable Energy Reviews* **2014**, 29, 325-335.

[10] Oshima, T.; Kajita, M., Development of Sodium-Sulfur Batteries. *International Journal of Applied Ceramic Technology* **2004**, 1, 269-276.

[11] Li, W.; Liu, J.; Yan, C., Reduced graphene oxide with tunable C/O ratio and its activity towards vanadium redox pairs for an all vanadium redox flow battery. *Carbon* **2013**, 55, 313-320.

[12] Kear, G.; Shah, A. A.; Walsh, F. C., Development of the all-vanadium redox flow battery for

energy storage: a review of technological, financial and policy aspects. *International Journal of Energy Research* **2012**, 36, 1105-1120.

[13] Parasuramana, A.; Lim, T. M.; Menictas, C.; Skyllas-Kazacos, M., Review of material research and development for vanadium redox flow battery applications. *Electrochimica Acta*, **2013** 101, 27-40.

[14] Li, B.; Gu, M.; Nie, Z.; Shao, Y.; Luo, Q.; Wei, X.; Li, X.; Xiao, J.: Wang, C.; Sprenkle, V.; Wang, W., Bismuth nanoparticle decorating graphite felt as a high-performance electrode for an all-vanadium redox flow battery. *Nano Letters*, **2013** 13, 1330-1335.

[15] You, D.; Zhanga, H.; Chena, J., A simple model for the vanadium redox battery. *Electrochimica Acta* **2009**, 54, 6827-6836.

[16] Jia, C.; Liu, J.; Yan, C., A significantly improved membrane for vanadium redox flow battery., *Journal of Power Sources* **2010**, 195, 4380-4383.

[17] Hueso, K. B; Armand, M.; Rojo, T., High temperature sodium batteries: status, challenges and future trends. *Energy Environmental Science* **2013**, 6, 734-749.

[18] Yamada, A.; Chung, S. C.; Hinokuma, K., Optimized LiFePO4 for lithium battery cathodes. *Journal of The Electrochemical Society* **2001**, 148, A224-A229.

[19] Chan, C. K.; Peng, H.; Liu, G.; McIlwrath, K.; Zhang, X. F.; Huggins, R. A.; Cui, Y., High-performance lithium battery anodes using silicon nanowires. *Nature Nanotechnology* **2008**, 3, 31-35.

[19] Lou, X. W.; Deng, D.; Lee, J. Y.; Feng, J.; Archer, L. A., Self-supported formation of needlelike Co_3O_4 nanotubes and their application as lithium-ion battery electrodes. *Advanced Materials* **2008**, 20, 258-262.

[20] Wang, D.; Choi, D.; Li, J.; Yang, Z.; Nie, Z.; Kou, R.; Hu, D.; Wang, C.; Saraf, L. V.; Zhang, J.; Aksay, I. A.; Liu, J., Self-assembled TiO_2–graphene hybrid nanostructures for enhanced Li-ion insertion. *ACS Nano* **2009**, 3, 907-914.

[21] Han, S.; Han, S.; Sezaki, K., Development of an optimal vehicle-to-grid aggregator for frequency regulation. *IEEE Transactions on Smart Grid* **2010**, 1, 65-72.

[22] Parka, M.; Zhanga, X.; Chunga, M.; Less, G. B.; Sastry, A. M.; A review of conduction phenomena in Li-ion batteries. *Journal of Power Sources* **2010**, 195, 7904-7929.

[23] Ma, J.; Wang, C.; Wroblewski, S., Kinetic characteristics of mixed conductive electrodes for lithium ion batteries. *Journal of Power Sources* **2007**, 164, 849-856.

[24] Bradwell, D. J.; Kim, H.; Sirk, A. H.; Sadoway, D. R., Magnesium−antimony liquid metal battery for stationary energy storage. *Journal of The American Chemical Society* **2012**, 134, 1895-1897.

[25] Fujiwaraa, S.; Inaba, M.; Tasaka, A., New molten salt systems for high temperature molten salt batteries: Ternary and quaternary molten salt systems based on LiF–LiCl, LiF–LiBr, and LiCl–LiBr. *Journal of The Power Sources* **2011**, 196, 4012-4018.

[25] Hoopes, W., Electrolytically-refined aluminum and articles made therefrom. *U.S. Patent 1,534,315*, **1925**.

[26] Cairns, E. J.; Crouthamel, C. E.; Fischer, A. K.; Foster, M. S.; Hesson, J. C., Galvanic cells with fused salts. *Argonne National Laboratory: Chicago* **1967**, ANL-7316, 27-85.

[27] Kim, H.; Boysen, D. A.; Newhouse, J. M.; Spatocco, B. L.; Chung, B.; Burke, P. J.; Bradwell, D. J.; Jiang, K.; Tomaszowska, A. A.; Wang, K.; Wei, W.; Ortiz, L. A.; Barriga, S. A.; Poizeau, S. M.; Sadoway, D. R., Liquid metal batteries: past, present, and future. *Chemical Reviews* **2013**, 113, 2075-2099.

[28] Bard, A. J.; Parsons, R.; Jordan, J., Standard Potentials in Aqueous Solution. *Marcel Dekker: New York* **1985**, 237-762.

[29] Bredig, M. A.; Bronstein, H. R.; Smith. Jr, W. T., Miscibility of liquid metals with salts. II. the potassium-potassium fluoride and cesium-cesium halide systems. *Journal of The American Chemical Society* **1955**, 77, 1454-1458.

[30] Bredig, M. A.; John son, J. W.; Smith. Jr, W. T., Miscibility of liquid metals with salts. I. the sodium-sodium halide systems. *Journal of The American Chemical Society* **1955**, 77, 307-312.

[31] Bredig, M. A.; Bronstein, H. R., Miscibility of liquid metals with salts. IV. The sodium-sodium halide systems at high temperature. *The Journal of Physical Chemistry* **1960**, 64, 64-67.

[32] Dworkin, A. S.; Bronstein, H. R.; Bredig, M. A., Miscibility of metals with salts. VI. Lithium-

lithium halide systems. *The Journal of Physical Chemistry* **1962**, 66, 572-573.

[33] Ouchi, T.; Sadoway, D. R., Corrosion of positive current collector in Li||Sb-Pb liquid metal battery for grid-scale energy storage. *The Electrochemical Society Meeting Abstract* **2014**.

[34] Conway, B. E.; Pell, W. G.;Liu, T.-C., Diagnostic analyses for mechanisms of self-discharge of electrochemical capacitors and batteries. *Journal of Power Sources* **1977**, 65, 53-59.

[35] Daou, T. J.; Pourroy, G.; Bégin-Colin, S.; Grenèche, J. M.; Ulhaq-Bouillet, C.; Legaré, P.; Bernhardt, P.; Leuvrey, C.; Rogez, G., Hydrothermal synthesis of monodisperse magnetite nanoparticles. *Chemistry of Materials* **2006**, 18, 4399-4404.

[36] Baruwati, B.; Kumar, D. K.; Manorama, S. V., Hydrothermal synthesis of highly crystalline ZnO nanoparticles: a competitive sensor for LPG and EtOH. *Sensors and Actuators B* **2006**, 119, 676-682.

[37] Chiu, H.-C.; Yeh, C,-S., Hydrothermal synthesis of SnO_2 nanoparticles and their gas-sensing of alcohol. *The journal of Physical Chemistry C* **2007**, 111, 7256-7259.

[38] Jeon, S.; Braun, P. V., Hydrothermal synthesis of Er-doped luminescent TiO_2 nanoparticles. *Chemistry of Materials* **2003**, 15, 1256-1263.

[39] Ley, K. L.; Krumpelt, M.; Kumar, R.; Meiser, J. H.; Bloomc, I., Glass-ceramic sealants for solid oxide fuel cells: part I. physical properties. *Journal of Materials Research* **1996**, 11, 1489-1493.

[40] Sohn, S.-B.; Choi, S.-Y., Suitable glass-ceramic sealant for planar solid-oxide fuel cells. *Journal of The American Ceramic Society* **2004**, 87, 254-260.

[41] Xiao, H.; Reitz, T., Anode-supported solid oxide fuel cells with thin film electrolyte for operation at reduced temperatures. *Electrochemical Society Transactions* **2006**, 1, 201-208.

[42] Whittingham, M. S.; Huggins, R. A., Measurement of sodium ion transport in beta alumina using reversible solid electrodes. *The Journal of Chemical Physics* **1971**, 54, 414-416.

[43] Engstrom, H.; Bates, J.B.; Brundage, W.E.; Wang, J.C., Ion conductivity of sodium beta"-alumina. *Solid State Ionics* **1981**, 2, 265-276.

[44] Yao, Y.-F.; Kummer, J. T., Ion exchange properties of and rates of ionic diffusion in beta-alumina. *Journal of Inorganic and Nuclear Chemistry* **1967**, 29, 2453-2475.

[45] Lu, X.; Li, G.; Kim, J. Y.; Mei, D.; Lemmon, J. P.; Sprenkle, V. L.; Liu, J., Liquid-metal electrode to enable ultra-low temperature sodium–beta alumina batteries for renewable energy storage. *Nature Communication* **2014**, 4578.

[46] Janz, G.J., Molten salt handbook. *Academic Press* **1967**.

[47] Janz, G. J.; Tomkins, R. P. T.; Allen, C. B.; Downey Jr., J. R.; Garner, G. L.; Krebs, U.; Singer, S. K., Molten salts: volume 4, part 2, chlorides and mixtures—electrical conductance, density, viscosity, and surface tension data., *Journal of Physical and Chemical Reference Data* **1975**, 4, 871-1178.

[48] Newhouse, J. M., Modeling the operating voltage of liquid metal battery cells. *Massachusetts Institute of Technology* **2014**, 48-49.

[49] Spatocco, B. L.; Ouchi, T.; Lambotte, G.; Burke, P. J.; Sadoway, D. R., Low-temperature molten salt electrolytes for membrane-free sodium metal batteries. *Journal of The Electrochemical Society* **2015**, 162, A2729 – A2736.

[50] Konys, J.; Borgstedt, H. U., The product of the reaction of alumina with lithium metal., *Journal of Nuclear Materials* **1985**, 131, 158-161.

[51] Wang, K.; Jiang, K.; Chung, B.; Ouchi, T.; Burke, P. J.; Boysen, D. A.; Bradwell, D. J.; Kim, H.; Muecke, U.; Sadoway, D. R., Lithium–antimony–lead liquid metal battery for grid-level energy storage. *Nature* **2014**, 514, 348-350.

[52] Li, H.; Wang, K.; Cheng, S.; Jiang, K., High performance liquid metal battery with environmentally friendly antimony−tin positive electrode. *ACS applied materials & Interfaces* **2016**, 8, 12830-12835.

[53] Sfriebel, K. A.; Deng, C. Z.; Wen, S. J.; Cairns, E. J., Electrochemical behavior of LiMn2O4 and LiCoO2 thin films produced with pulsed laser deposition. *Journal of The Electrochemical Society* **1996**, 143, 1821-1827.

[54] Ning, X.; Phadke, S.; Chung, B.; Yin, H.; Burke, P.; Sadoway, D. R., Self-healing Li-Bi liquid metal battery for grid-scale energy storage. *Journal of Power Sources* **2015**, 275, 370-376.

[55] Bredig, M. A., Mixtures of metals with molten salts. *Oak ridge national laboratory* **1963**, ORNL-3391.

10. Acknowledgements